Deep-Sea Research II 56 (2009) 554–577

Contents lists available at ScienceDirect

Deep-Sea Research II

journal homepage: www.elsevier.com/locate/dsr2

Climatological mean and decadal change in surface ocean pCO_2, and net sea–air CO_2 flux over the global oceans

Taro Takahashi [a,*], Stewart C. Sutherland [a], Rik Wanninkhof [b], Colm Sweeney [c], Richard A. Feely [d], David W. Chipman [e], Burke Hales [f], Gernot Friederich [g], Francisco Chavez [g], Christopher Sabine [d], Andrew Watson [h], Dorothee C.E. Bakker [h], Ute Schuster [h], Nicolas Metzl [i], Hisayuki Yoshikawa-Inoue [j], Masao Ishii [k], Takashi Midorikawa [k], Yukihiro Nojiri [l], Arne Körtzinger [m], Tobias Steinhoff [m], Mario Hoppema [n], Jon Olafsson [o], Thorarinn S. Arnarson [o], Bronte Tilbrook [p], Truls Johannessen [q], Are Olsen [q], Richard Bellerby [q], C.S. Wong [r], Bruno Delille [s], N.R. Bates [t], Hein J.W. de Baar [u]

[a] Lamont-Doherty Earth Observatory, Columbia University, 61 Route 9W, PO Box 1000, Palisades, NY 10964-8000, USA
[b] Atlantic Oceanographic and Meteorological Laboratory, National Oceanographic and Atmospheric Administration, Miami, FL, USA
[c] Earth System Research Laboratory, National Oceanographic and Atmospheric Administration, Boulder, CO, USA
[d] Pacific Marine Environmental Laboratory, National Oceanographic and Atmospheric Administration, Seattle, WA, USA
[e] 103 Reach Road, Harpswell, ME, USA
[f] College of Oceanic and Atmospheric Sciences, Oregon State University, Corvallis, OR, USA
[g] Monterey Bay Aquarium Research Institute, Moss Landing, CA, USA
[h] School of Environmental Sciences, University of East Anglia, Norwich, UK
[i] Laboratoire d'Océanographie et du Climat, LOCEAN/IPSL, CNRS, Université Pierre et Marie Curie, Paris, France
[j] Graduate School of Environmental Earth Science, Hokkaido University, Sapporo, Japan
[k] Meteorological Research Institute, Tsukuba, Japan
[l] National Institute for Environmental Studies, Tsukuba, Japan
[m] Leibniz Institute of Marine Sciences, Kiel, Germany
[n] Alfred Wegener Institute, Bremerhaven, Germany
[o] Marine Research Institute and University of Iceland, Reykjavik, Iceland
[p] Wealth from Oceans, CSIRO National Research Flagship, and the Antarctic Climate and Ecosystem Cooperative Research Center, Hobart, Australia
[q] Bjerknes Centre for Climate Research, University of Bergen, Norway
[r] Institute of Ocean Sciences, Fisheries and Oceans Canada, Sidney, B.C., Canada
[s] Université de Liege, Liege, Belgium
[t] Bermuda Institute of Ocean Studies, Bermuda
[u] Royal Netherlands Institute of Sea Research, Den Burg, The Netherlands

ARTICLE INFO

Available online 16 December 2008

Keywords:
Carbon dioxide
Partial pressure
Surface ocean
Global ocean
Sea–air flux

ABSTRACT

A climatological mean distribution for the surface water pCO_2 over the global oceans in non-El Niño conditions has been constructed with spatial resolution of 4° (latitude) × 5° (longitude) for a reference year 2000 based upon about 3 million measurements of surface water pCO_2 obtained from 1970 to 2007. The database used for this study is about 3 times larger than the 0.94 million used for our earlier paper [Takahashi et al., 2002. Global sea–air CO_2 flux based on climatological surface ocean pCO_2, and seasonal biological and temperature effects. Deep-Sea Res. II, 49, 1601–1622]. A time-trend analysis using deseasonalized surface water pCO_2 data in portions of the North Atlantic, North and South Pacific and Southern Oceans (which cover about 27% of the global ocean areas) indicates that the surface water pCO_2 over these oceanic areas has increased on average at a mean rate of 1.5 μatm y^{-1} with basin-specific rates varying between 1.2 ± 0.5 and 2.1 ± 0.4 μatm y^{-1}. A global ocean database for a single reference year 2000 is assembled using this mean rate for correcting observations made in different years to the reference year. The observations made during El Niño periods in the equatorial Pacific and those made in coastal zones are excluded from the database.

Seasonal changes in the surface water pCO_2 and the sea-air pCO_2 difference over four climatic zones in the Atlantic, Pacific, Indian and Southern Oceans are presented. Over the Southern Ocean seasonal ice zone, the seasonality is complex. Although it cannot be thoroughly documented due to the limited extent of observations, seasonal changes in pCO_2 are approximated by using the data for under-ice waters during austral winter and those for the marginal ice and ice-free zones.

* Corresponding author.
E-mail address: taka@ldeo.columbia.edu (T. Takahashi).

0967-0645/$ - see front matter
doi:10.1016/j.dsr2.2008.12.009

The net air–sea CO_2 flux is estimated using the sea–air pCO_2 difference and the air–sea gas transfer rate that is parameterized as a function of (wind speed)^2 with a scaling factor of 0.26. This is estimated by inverting the bomb ^{14}C data using Ocean General Circulation models and the 1979–2005 NCEP-DOE AMIP-II Reanalysis (R-2) wind speed data. The equatorial Pacific (14°N–14°S) is the major source for atmospheric CO_2, emitting about +0.48 Pg-C y^{-1}, and the temperate oceans between 14° and 50° in the both hemispheres are the major sink zones with an uptake flux of −0.70 Pg-C y^{-1} for the northern and −1.05 Pg-C y^{-1} for the southern zone. The high-latitude North Atlantic, including the Nordic Seas and portion of the Arctic Sea, is the most intense CO_2 sink area on the basis of per unit area, with a mean of −2.5 tons-C month^{-1} km^{-2}. This is due to the combination of the low pCO_2 in seawater and high gas exchange rates. In the ice-free zone of the Southern Ocean (50°–62°S), the mean annual flux is small (−0.06 Pg-C y^{-1}) because of a cancellation of the summer uptake CO_2 flux with the winter release of CO_2 caused by deepwater upwelling. The annual mean for the contemporary net CO_2 uptake flux over the global oceans is estimated to be -1.6 ± 0.9 Pg-C y^{-1}, which includes an undersampling correction to the direct estimate of -1.4 ± 0.7 Pg-C y^{-1}. Taking the pre-industrial steady-state ocean source of 0.4 ± 0.2 Pg-C y^{-1} into account, the total ocean uptake flux including the anthropogenic CO_2 is estimated to be -2.0 ± 1.0 Pg-C y^{-1} in 2000.

1. Introduction

Recent rapid accumulation of CO_2 in the atmosphere is one of the major environmental concerns because of its potential effects on the future global climate. Anticipated warming and associated environmental changes including sea-level rise would adversely affect the socio-economic stability of human society and global terrestrial–marine ecosystems. The results of various independent lines of study show that the present net global ocean CO_2 uptake (not including the pre-industrial steady-state flux) is 1.5–2.0 Pg-C y^{-1} (Pg = Peta grams = 10^{15} g = 1 Giga ton), which corresponds to about 25% of the industrial emissions of about 7 Pg-C y^{-1} (Bender et al., 2005; Gloor et al., 2003; Gruber and Sarmiento, 2002; Gurney et al., 2004; Jacobson et al., 2007a, b; Keeling and Garcia, 2002; Mikaloff-Fletcher et al., 2006; Patra et al., 2005; Quay et al., 2003; Sabine et al., 2004; Sarmiento et al., 2000; Takahashi et al., 2002). Accurate assessment of the sea–air CO_2 flux and its time–space variability is important information for the improvement of our understanding of the global carbon cycle and the prognosis for the future atmospheric CO_2 concentration. In this paper, we summarize the measurements of partial pressure of CO_2 in surface waters made 1970–2006 by a large number of international investigators over the global oceans and present estimates for the sea–air CO_2 flux.

The difference between the partial pressure of CO_2 in seawater and that in the overlying air, $\Delta pCO_2 = [(pCO_2)_{sw} - (pCO_2)_{air}]$, is the thermochemical driving potential for the net transfer of CO_2 across the sea surface. For example, when $(pCO_2)_{air}$ is greater than $(pCO_2)_{sw}$, ΔpCO_2 is negative and atmospheric CO_2 is taken up by the seawater. The net CO_2 flux across sea surface can be estimated by multiplying the ΔpCO_2 by the CO_2 gas transfer coefficient, which depends primarily on the degree of turbulence near the interface. Using this principle, the first set of global surface water pCO_2 data, consisting of about 0.24 million pCO_2 measurements, was assembled and the climatological mean distributions of ΔpCO_2 and sea–air CO_2 flux were estimated (Takahashi et al., 1997) using the time–space interpolation method based on a 2-dimensional diffusion–advection transport equation (Takahashi et al., 1995). In the course of the following several years, the database were more than tripled in size to about 0.94 million measurements by 2002, and the second improved version that included the climatological mean monthly distribution of surface water pCO_2 and sea–air flux in the reference year 1995 was published (Takahashi et al., 2002). The database have since been increased by another three-fold to 3 million $(pCO_2)_{sw}$ measurements. As a result, we have been able to obtain a more reliable estimate for interannual changes in surface water pCO_2. This paper presents the new results for the climatological mean distribution of surface water pCO_2 and net sea–air CO_2 flux over the global oceans in the reference year of 2000 representing mean non-El Niño conditions.

2. Measurements of surface water pCO_2 and database

2.1. Data sources and database

The database used for this study consists of about 3.0 million measurements of surface water pCO_2 obtained since the early 1970s. About 0.2 million measurements made in the equatorial Pacific, 10°N–10°S, during the five El Niño periods (1982–1983, 1986–1987, 1991–1994, 1997–1998, 2002–2003 and 2004–2005) and about 0.2 million made in the coastal waters (within about 200 km from the shore) are excluded from the total database of 3.4 million. The remaining 3.0 million $(pCO_2)_{sw}$ values used for the analysis represent open-ocean environments during non-El Niño conditions. This is supplemented by an equal number of other associated data such as SST and salinity. The earlier publications that describe the data are listed in Takahashi et al. (1993, 2002), and the original data files for more recent observations are available from the authors of this paper. Since investigators processed the field observations somewhat differently, we have recomputed all the data using the procedures described below in order to produce a uniform database. The entire database including the coastal and El Niño period equatorial Pacific data (Takahashi et al., 2008) are available at the Carbon Dioxide Information and Analysis Center at the Oak Ridge National Laboratory, Oak Ridge, TN (LDEO database (NDP-088) at http://cdiac.ornl.gov/oceans/doc.html).

Although pCO_2 may be computed using TCO_2, alkalinity and/or pH, it depends on the choice of dissociation constants used. Therefore, we accepted in the database only the pCO_2 values measured directly using the air–water equilibration method, in which two or more standard gas mixtures (not counting pure nitrogen or CO_2-free air) were used for analyzer calibrations.

2.2. Method for measurements

The $(pCO_2)_{sw}$ data used in this study were determined using a turbulent water–air equilibration method modified from the basic designs developed during the 1957–1959 International Geophysical Year (Takahashi, 1961; Keeling et al., 1965; Broecker and Takahashi, 1966), or of the membrane-equilibrator method (Hales et al., 2004). A volume of carrier gas is equilibrated with seawater

(closed or continuously flowing), and the concentration of CO_2 in the equilibrated carrier gas is measured using a CO_2 gas analyzer, either by infrared CO_2 absorption or gas chromatographic analyses. The analyzers are calibrated using two or more reference gas mixtures, of which the CO_2 molar mixing ratios are traceable to either the WMO standards maintained by C.D. Keeling or the reference gases certified by the Earth System Research Laboratory of NOAA. When a dried carrier gas is analyzed, the pCO_2 in seawater at equilibration temperature, T_{eq}, is computed using

$$(pCO_2)_{sw} = XCO_2(P_{eq} - P_w) \quad (1)$$

where XCO_2 is the mole fraction of CO_2 in dry air; P_{eq} is the total pressure of carrier gas in the equilibration chamber; and P_w is the water vapor pressure at the temperature of equilibration, T_{eq}, and salinity. When the CO_2 mixing ratios in the wet carrier gas is determined, P_w is set at zero. When an equilibrator is located in an enclosed shipboard laboratory and is open to the room air, P_{eq} is the ambient pressure in the laboratory. In some data sets, P_{eq} is not reported for an equilibrator operated in an enclosed space. In such cases, P_{eq} is assumed to be the reported barometric pressure at sea surface plus 3 mb, that represents an overpressure normally maintained inside a ship. This correction increases the $(pCO_2)_{sw}$ value by about 1 μatm.

To correct the $(pCO_2)_{sw}$ measured at T_{eq} to the in situ seawater temperature, $T_{in\ situ}$, a constant-chemistry temperature effect, $(\partial \ln pCO_2/\partial\ T) = 0.0433 - 8.7 \times 10^{-5} T$ (°C), which was determined for a North Atlantic surface water sample (Takahashi et al., 1993), is used. Eq. (2) is an integrated form of the equation above:

$$(pCO_2)_{sw} \text{ at } T_{in\ situ} = [(pCO_2)_{sw} \text{ at } T_{eq}]\,\mathrm{Exp}\{0.0433(T_{in\ situ} - T_{eq}) - 4.35 \times 10^{-5}[(T_{in\ situ})^2 - (T_{eq})^2]\} \quad (2)$$

In our previous publication (Takahashi et al., 2002), a mean coefficient of 0.0423 °C^{-1} (Takahashi et al., 1993) was used instead of Eq. (2). If $(T_{in\ situ} - T_{eq})$ is less than 2 °C, Eq. (2) yields pCO_2 values virtually indistinguishable from the previous ones. Since temperature changes for continuous underway systems are commonly less than this, the corrections made using the constant coefficient do not require changes. Only those measured for discrete water samples are subject to change up to about 3 μatm. For the reasons discussed in Section 2.3, we take the reported "bulk" water temperature as $T_{in\ situ}$ to represent the sea-surface condition. The average precision of individual pCO_2 measurements thus obtained is estimated to be ±3 μatm at a reported "bulk" water temperature.

Since the data reported by the participating groups had been processed using different computational schemes, all the data are recomputed using Eqs. (1) and (2) in order to remove biases. In the calculation, CO_2 gas is treated as ideal in the range of pressures encountered in this study, and the effects of non-ideal mixing behaviors of CO_2 molecules in air due to CO_2–H_2O–N_2–O_2 molecular interactions are neglected since they are small (<1 μatm) and are inferred from correlations among the heat of mixing and other thermodynamic parameters for various molecular species (Weiss and Price, 1980).

2.3. Temperature of ocean water

The upper several meters of the ocean are thermally stratified depending upon heat balance and turbulence. Since pCO_2 in seawater depends sensitively on temperature, we need to select a $T_{in\ situ}$ in Eq. (2), that is critical to the sea–air CO_2 gas transfer. In the skin layer regime (<500 μm), where conductive and diffusive heat transfer processes are dominant, the layer is cooled due to evaporation; in the sub-skin regime (~1 cm to a few meters), where diffusive and viscous processes are important, the water is warmed by short-wave solar radiation during the day time; and the bulk mixing layer (a few to several meters) is governed primarily by turbulent mixing. Donlon et al. (2002) compared the bulk water temperatures measured at a depth of 5 m concurrently with the mean skin temperature observations using a shipboard infrared radiometer during six cruises between 50°N and 50°S in the Atlantic and Pacific Oceans. They observed that, at wind speeds exceeding 6 m s^{-1}, the skin temperatures were cooler than the bulk water temperatures (measured at 5 m) by -0.17 ± 0.07 °C for both the day- and night-time conditions. At lower wind speeds, skin temperatures of 2 °C or more warmer than bulk temperatures were observed during day-time, but not during night-time.

Sarmiento and Sundquist (1992) and Robertson and Watson (1992) proposed that, since skin layer of the oceans is a few tenths of degree cooler than the bulk water, the skin layer pCO_2 should be lower by as much as 1% than that at the bulk water temperature, thus increasing the air-to-sea CO_2 flux by as much as 30% (or 0.1–0.7 Pg-C y^{-1}). On the other hand, McGillis and Wanninkhof (2006) pointed out that, since molecular diffusivities for gases and salt are nearly two orders of magnitude smaller than the thermal diffusivity, the thickness of the diffusive layer for gases should be an order of magnitude smaller than that for the thermal diffusive layer. Hence, the difference between the (CO_2)aq (and hence pCO_2) in the skin- and sub-skin layers should be an order of magnitude smaller than that estimated on the basis of the thermal skin layer thickness. The effect of skin cooling on pCO_2, therefore, should be much smaller than previously proposed. Furthermore, Zhang and Cai (2007) consider that, as a result of smaller salt diffusivity than thermal diffusivity in seawater, the skin cooling caused by evaporation may be accompanied with a much thinner salty-skin layer. Since the pCO_2 of seawater decreases with cooling and increases with salinity ($\partial \ln pCO_2/\partial \ln Sal = 0.94$, Takahashi et al., 1993), the effect of skin cooling should be nearly cancelled by that of salty skin. Since the skin layer thickness decreases inversely proportional to wind speed (Saunders, 1967; Fairall et al., 1996), its effect on pCO_2 should be reduced over high wind speed areas of the oceans (such as the southern high wind belt 40–55°S). Therefore, the effect of skin layer cooling on seawater pCO_2 is considered to be negligibly small.

In addition to the effect of skin layer cooling, solar heating affects the temperature of the upper few meters of tropical oceans (Fairall et al., 1996). Satellite-borne microwave measurements show that, over tropical regions under low wind speed conditions, the day-time temperatures of the upper few meters of water exceed the bulk water temperatures (those assembled by Reynolds and Smith (1994)) as much as 2.8 °C (Gentemann et al., 2003). The day-time warming would influence the net daily sea–air flux of CO_2 especially in tropical oceans (McNeil and Merlivat, 1996; Ward et al., 2004). On the other hand, for this study, most of the pCO_2 were measured during day and night continuously for a depth range of 1–7 m, and the pCO_2 and bulk water temperature data are averaged over a $4^\circ \times 5^\circ$ box area without differentiating the day- and night-time measurements. Hence, the pCO_2 bias resulting from the day-time warming is considered minimal.

As discussed above, the pCO_2 that represents the interface layer with the atmosphere cannot be defined unequivocally on the basis of the measurements in our database. Nevertheless, based on the available information, we judge that the effect of thermal skin layer on pCO_2 is negligibly small, and that the bias due to diurnal temperature changes is minimized by the averaging of large number of day- and night-time measurements. In this study, therefore, the pCO_2 value measured at the "bulk" water temperature is taken as that for the sea-surface value. As the surface-layer effects should become further clarified in the future, they should be taken into consideration in order to reduce systematic errors in sea–air pCO_2 differences.

2.4. Atmospheric pCO_2

The atmospheric pCO_2, $(pCO_2)_{air}$, in the reference year 2000 is computed using:

$$(pCO_2)_{air} = XCO_2(P_{baro} - P_{sw}) \quad (3)$$

where P_{baro} is the barometric pressure at sea surface, and P_{sw} is the water vapor pressure at the temperature and salinity for mixed layer water. The following values are used: the weekly mean XCO_2 data in dry air from the GLOBALVIEW—CO_2 Database (2006); for P_{sw}, 100% humidity at SST (temperature of bulk mixed layer water) and surface water salinity from the NOAA's Atlas of Surface Marine Data (1994); and for P_{baro}, the climatological monthly mean barometric pressure at sea surface from the NCEP Reanalysis data (2001). The sea–air pCO_2 difference, ΔpCO_2, is then computed using

$$\Delta pCO_2 = [(pCO_2)_{sw} \text{ corrected to the year 2000}] - [(pCO_2)_{air} \text{ in 2000}] \quad (4)$$

Since CO_2 is assumed to be an ideal gas for both $(pCO_2)_{sw}$ and $(pCO_2)_{air}$, the small effects of non-ideality should cancel due to differencing for pCO_2. Positive ΔpCO_2 values indicate that the sea is a source for atmospheric CO_2, whereas negative values indicate that the sea is a sink.

It should be noted that, while the multi-decadal climatological mean for SST, sea-surface salinity and barometric pressure are nearly steady, the atmospheric and surface ocean pCO_2 have been changing over the study period due to emissions of anthropogenic CO_2. Accordingly, to obtain climatological mean distribution and mean for ΔpCO_2, $(pCO_2)_{sw}$ values that were measured in different years must be corrected to a single reference year. In this paper, the year 2000 is chosen as the reference year, since it is close to the mean year for the pCO_2 data. Analytical precision for a single measurement of ΔpCO_2 is estimated to be about $\pm 4\,\mu atm$. However, since a box area often encompasses various oceanographic features (such as currents, eddies, upwelling and patchy biological activities) (e.g. Li et al., 2005), the uncertainty in mean ΔpCO_2 values is commonly dominated by $(pCO_2)_{sw}$ variations associated with these features.

2.5. Distribution of measurements

We choose a 4° (latitude) × 5° (longitude) spatial resolution for this study based primarily on the time–space density of the

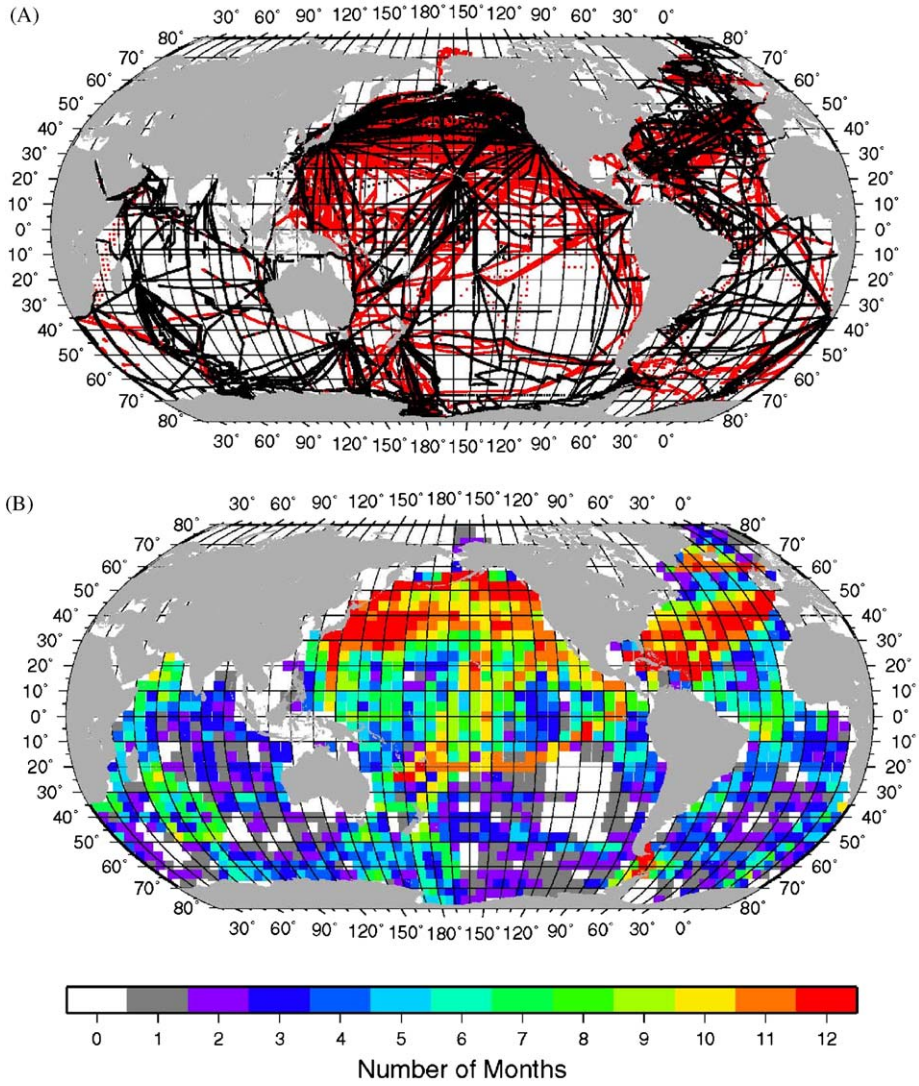

Fig. 1. (A) Sampling locations. The black dots indicate the measurements in the 0.94 M database used in Takahashi et al. (2002) and the red dots are new measurements added to the database (3.0 M) used in this study. (B) Number of months in each 4° × 5° box area where at least one surface water pCO_2 measurement has been made since the early 1970s. White areas have no measurements.

observations. While smaller box areas would help to resolve narrow oceanographic features such as the Gulf Stream and equatorial currents, they would reduce the number of observations made in a box during different seasons and hence fail to define seasonal variation. Even at this box size, observations made in several years have to be combined to define seasonal variability. Multi-year composite maps summarizing the sampling locations and the number of months, in which at least one measurement was made since 1970 in each box, are shown in Figs. 1A and B. The latter map shows that, of a total of 1759 boxes, about 30% of the boxes have measurements spanning 6 or more months, and 50% of the boxes have measurements spanning 3 or less months. While most boxes in the Northern Hemisphere have observations in 6 or more months, many in the Southern Hemisphere oceans south of 20°S have data only in 3 or less months. The Drake Passage areas that are being investigated as part of the Long Term Ecosystem Research (LTER) program along the Antarctic Peninsula are the only southern high-latitude boxes that have 12-month data.

3. Normalization of data to a reference year

The surface water pCO_2 varies seasonally and from year to year due to changes in biological and physical conditions. In addition, it changes in response to increasing atmospheric pCO_2, and over a 30-year period, it could increase as much as 45 μatm, if seawater were equilibrated with the atmosphere. Therefore, the measurements made in different years need to be corrected to a single reference year in order to eliminate biases due to the sampling year and to obtain a climatological mean distribution. In light of the improved observations, the previous procedures used for Takahashi et al. (2002) need to be revised. In this section, the rates of pCO_2 change in various areas of the global oceans will be examined first, and the new methods that are used to normalize pCO_2 data to the single reference year 2000 will be presented. The differences between the pCO_2 values in Takahashi et al. (2002) and this study will be discussed in Section 5.3.

3.1. Method of analysis for mean rate of pCO_2 change in surface waters

Bates (2001) measured the carbonate chemistry parameters at the Bermuda Atlantic Time-Series Study (BATS) station (31°5′N and 64°10′W) over the 10-year period from late 1989 to early 1998. A linear regression of the deseasonalized data yielded a mean rate of $1.4 \pm 1.1\ \mu atm\ y^{-1}$, which is indistinguishable from the mean atmospheric pCO_2 increase rate of $1.33\ \mu atm\ y^{-1}$ (see Bates, 2001, Fig. 3, p. 1514). Following this method, we estimate the mean rate of change for surface water pCO_2 in selected areas by linearly regressing deseasonalized mean monthly values. Because we do not have sufficient seasonal coverage in a large number of our $4^\circ \times 5^\circ$ boxes, we expand the scale of the boxes, in some cases to $5^\circ \times 10^\circ$, for this analysis.

An example for the deseasonalization procedure is shown in Fig. 2 using the data from an oceanic area 20–25°S and 165–175°E in the South Pacific (hereafter called "Vanuata" zone on the basis of islands located within this box). The box area is selected to have sufficient number of seasonal measurements, and, at the same time, to avoid geographic and oceanographic features such as the local effects of islands. Using the measurements made during 1993–1996, the seasonal changes are estimated on the basis of the monthly mean values (open circles) computed from the 4-year composite data. Values for months with no measurement (open squares) are estimated by a linear interpolation using adjacent mean monthly values. The difference between a monthly mean and the annual mean represents the correction to be applied for

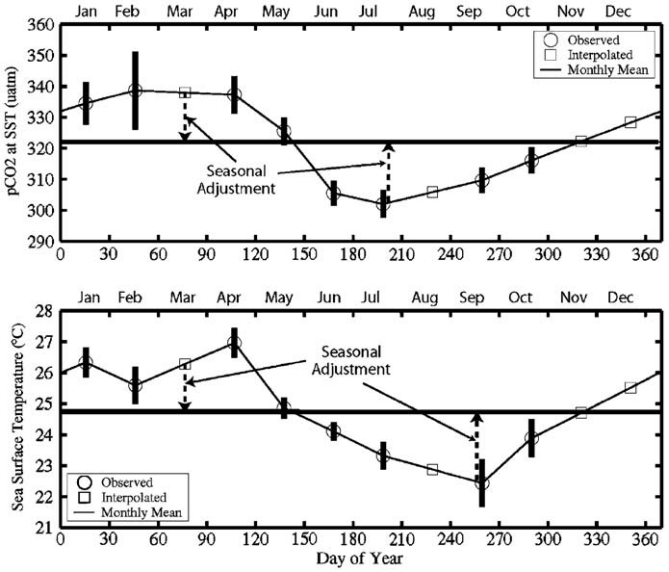

Fig. 2. Surface water pCO_2 and SST data obtained in the Vanuata area, 20–25°S and 165–175°E in the South Pacific in 1993–1996. The mean seasonal variability for the 4-year period is established assuming that the seasonal variations remained unchanged over this period. The open circles are monthly mean values and the error bars represent one standard deviation of observations. The values for months with no measurements are linearly interpolated using adjacent monthly mean values, and are shown with open squares. The heavy horizontal line indicates the annual mean. The differences between the monthly mean and the annual mean indicate the seasonal corrections used for deseasonalization.

deseasonalization of the monthly mean. Assuming that the seasonal variability and hence the deseasonalization corrections remain unchanged with time, the monthly mean values obtained for years outside the 4-year period are corrected to obtain deseasonalized values.

The deseasonalized mean monthly values thus obtained are regressed linearly against time (year) to obtain the mean rate of change. Uncertainties for the rates of change are computed using

$$\pm[\sigma^2/(\Sigma(X_i^2) - N(X_{mean})^2)]^{1/2} \quad (5)$$

where $\sigma^2 = [(\Sigma(Y_i - aX_i - b)^2)/(N-2)]$ is the variance around the fitted equation $Y = aX + b$, and Y is $(pCO_2)_{sw}$ or SST and X is year. In this study, the amplitude and phase for seasonal changes estimated for each box area are assumed to be unchanged throughout the 30-year period. The magnitude of deseasonalization corrections and hence the rate of pCO_2 change are affected by interannual changes in the seasonal variability, especially when seasonal amplitudes are large as seen in the high-latitude areas (e.g., the Bering Sea, Fig. 5C). This should introduce an additional uncertainty to the mean rate of pCO_2 change estimated using the procedures described above. Hence, the uncertainty computed using Eq. (5) should be considered a minimum estimate.

3.2. North Atlantic Ocean

Of the 5°(latitude) × 10° (longitude) boxes in the North Atlantic, 37 are found to have a sufficient number of seasonal pCO_2 measurements over sufficiently long period to allow determination of the decadal mean rate of change. Fig. 3 shows examples for the time-trend data in the three box areas in the North Atlantic: the Irminger Sea, north of the Azores and east of Barbados. The large variability seen in higher latitude areas is attributed largely to large seasonal changes in temperature, intense biological activities and mixing as well as complex current structures such as the Arctic and warm North Atlantic Currents.

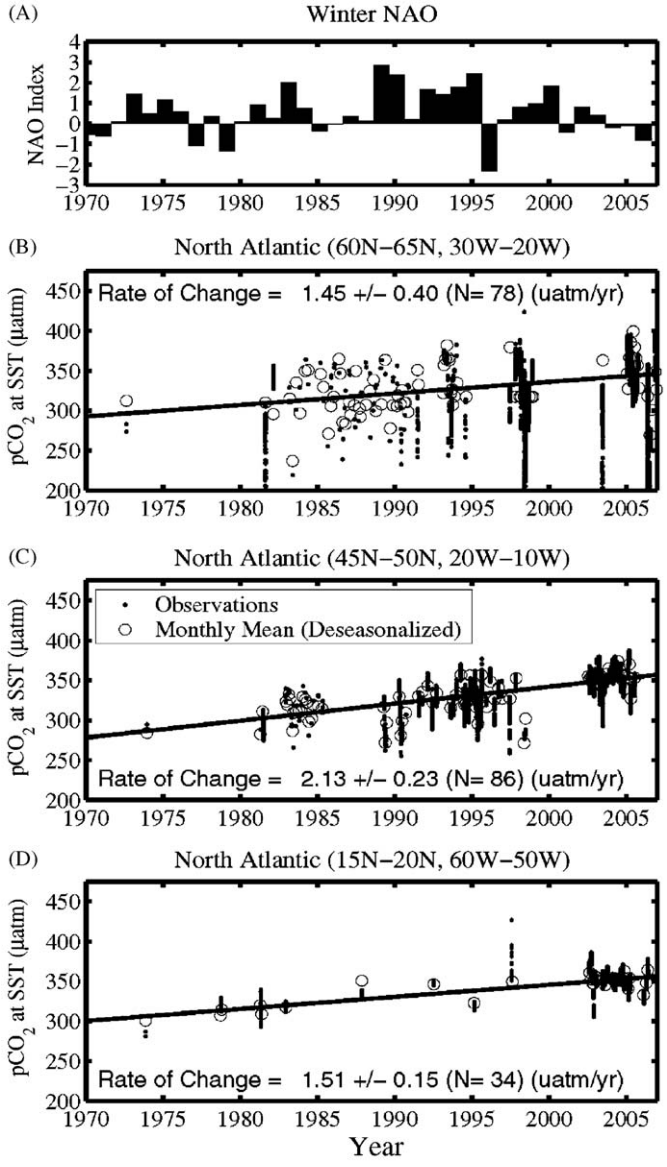

Fig. 3. (A) Winter-time NAO index, (B) temporal change in the surface water pCO_2 observed in the Irminger Sea (60–65°N; 30–20°W), (C) north of the Azores (45–50°N; 20–10°W) and (D) east of Barbados (15–20°N; 60–50°W). Black dots indicate the observed values, and the open circles indicate the deseasonalized mean monthly values. The solid line shows a linear regression, and the mean rate of change is shown in each panel. N is the number of monthly mean values used.

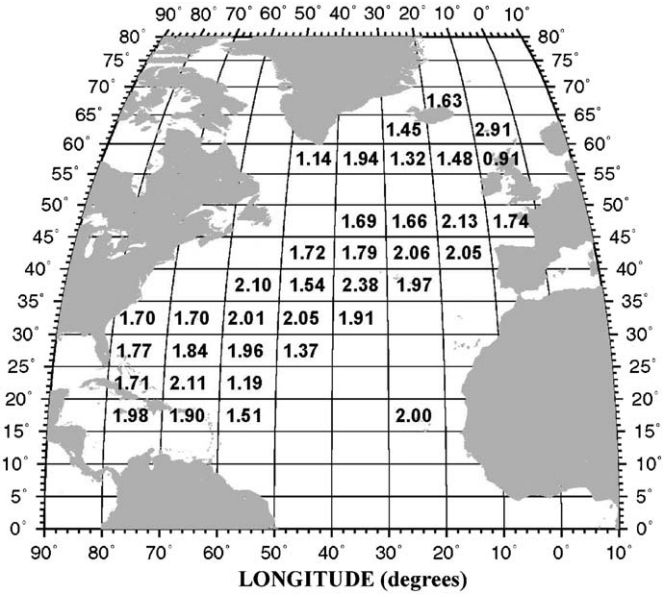

Fig. 4. Mean rates of increase during 1970–2007 in surface water pCO_2 in 5° latitude × 10° longitude box areas in the North Atlantic. The number in each box indicates the rates in $\mu atm\,y^{-1}$. Uncertainties for the rates range between ±0.1 and ±0.6 $\mu atm\,y^{-1}$ depending upon the seasonal amplitude and the length of record in each box area.

Because of uneven time distribution of measurements, it is not possible to detect correlation of the pCO_2 with the winter NAO index (Fig. 3A).

Fig. 4 shows the mean rates of increase in surface water pCO_2 in 37 box areas over the North Atlantic. Regional differences in the rates are not obviously discernible. The mean for the 37 box areas (weighted with the reciprocal of the estimated errors in the mean slope, Eq. (5), and by the area of each box) is $1.8 \pm 0.4\,\mu atm\,y^{-1}$.

The mean rates of increase in surface water pCO_2 thus obtained in the North Atlantic and other published values are summarized in Table 1. Observations at BATS by Bates (2001) 1989–1998 and at BATS and Station S by Gruber et al. (2002) and Bates (2007), 1983–2003, constitute the most complete data sets in the western North Atlantic, and give a decadal mean rate of pCO_2 increase ranging from 1.4 to $1.67\,\mu atm\,y^{-1}$. Lefèvre et al. (2004) reconstructed pCO_2 values from 1982 to 1998 on a 1° × 1° grid for each month based on the pCO_2 values that were first normalized to a constant temperature and then smoothed and parameterized using latitude, longitude, SST and year of observations. They obtained a mean rate of $1.8\,\mu atm\,y^{-1}$ (uncertainty not reported in the paper) in the North Atlantic Drift area (50–58°N, 10–38°W) for the 17-year period. They also reported that the rate varied seasonally ranging from $4\,\mu atm\,y^{-1}$ during summer, when the mixed layer was shallowest and the vertical mixing rate was minimum, to $0\,\mu atm\,y^{-1}$ during fall, when the mixed layer deepened and deep waters were mixed into the mixed layer. Other estimates (Oudot et al., 1995; Omar et al., 2003; Olsen et al., 2006; Omar and Olsen, 2006; Corbière et al., 2007; Schuster and Watson, 2007) range from 2 to $4\,\mu atm\,y^{-1}$, but the sparse spatial and temporal coverage of these studies and the confounding effects of apparently seasonally-varying rates of increase makes direct comparison with this work difficult.

The results of previous studies listed in Table 1 show that the rate of increase in surface water pCO_2 varies geographically as well as within the time periods investigated. In contrast to the objectives of the previous studies, the aim of our analysis is to assess the basin-scale mean rate using 30+ years of observations by smoothing shorter time-scale variation. Hence, the published rates for specific areas and shorter time periods are not inconsistent with the basin-scale mean rate of increase of $1.8 \pm 0.4\,\mu atm\,y^{-1}$ representing a mean for the three decades. This mean rate is indistinguishable from that for the atmospheric pCO_2 of about $1.5\,\mu atm\,y^{-1}$ estimated for the 1972–2005 period using the GLOBALVIEW—CO_2 (2006).

3.3. North and equatorial Pacific Ocean

Takahashi et al. (2006) analyzed the surface water pCO_2 data obtained between 1970 and 2004 in the North Pacific, and estimated mean decadal rates of pCO_2 increase in 28 10° × 10° box areas located between 10° and 60°N. These 28 boxes were selected on the basis that the SST values measured concurrently with pCO_2 yielded mean rates of change consistent with those

Table 1
Mean rates of increase of surface water pCO_2 observed in the North Atlantic Ocean.

Locations	Lat. & Long.	pCO_2 rates ($\mu atm\,y^{-1}$)	Remarks
Barents Sea	73–80°N 20–58°E	1.4 ± 1	Difference between 1967 and 2000–2001; Omar et al. (2003)
Eastern subpolar North Atlantic	50–64°N 32–10°W	2.25 ± 0.75*	Reconstructed rate between 1972 and 1989; Omar and Olsen (2006)
E. Nordic seas	60–80°N 10°E–15°W	1.6–2.4* ±0.4	Difference between 1981 and 2003; TA & TCO_2; Olsen et al. (2006)
NE Atlantic (Newfoundland to Iceland)	53–62°N 20–45°W	1.8 Summer* 2.8 Winter*	1993–1997 and 2001–2004; TA & TCO_2; Corbière et al. (2007)
N. Atlantic Drift	50–58°N 10–38°W	$1.8\pm$? $4\,\mu atm\,y^{-1}$ for May–July; $0\,\mu atm\,y^{-1}$ for Oct.–Nov.	1982-98; pCO_2; Lefèvre et al. (2004)
N. Atlantic (UK to Caribbean)	20°N, 70°W–50°N, 5°W	$4.4\pm$?	Mean difference between 1994–95 and 2002–05; pCO_2; Schuster and Watson (2007)
BATS	31°N; 64°W	2.7 ± 1.9* 1.4 ± 1.1*	1988–1998; TA & TCO_2; linear fit to all data 1988–1998; linear fit to deseasonalized data; Bates (2001)
BATS & Stn. S	31–32°N	1.5 ± 0.1* 1.67 ± 0.28*	1983–2001; TA & TCO_2; Gruber et al. (2002) 1983–2003; TA & TCO_2; Bates (2007)
Eastern Eq. Atlantic	8°N–5°S 5–35°W	2.5–2.8	Mean difference between 1982 & 1992 French FOCAL pCO_2 data; Oudot et al. (1995)
N. Atlantic Basin	15–70°N 0–75°W	1.8 ± 0.4	1972–2006; pCO_2; This study Mean of the rates determined in 37 5°(lat.) × 10° (long.) box areas

"TA & TCO_2" and * indicate that pCO_2 in seawater was computed using the total alkalinity and total CO_2 concentration; and "pCO_2" indicates that it was measured directly.

obtained from the extensive database of Reynolds et al. (2003) for the mixed layer bulk water temperature (SST). The rates range between 0.5 and 2 $\mu atm\,y^{-1}$ for the open North Pacific. The lower rates (0.5–0.7 $\mu atm\,y^{-1}$) that were observed in the Kuroshio Current areas could be due to the outflow from the East China Sea. Although the pCO_2 rates varied geographically, an open-ocean average is $1.2\pm0.4\,\mu atm\,y^{-1}$. Fig. 5 shows the time trends observed in three North Pacific box areas, which include, respectively, the Weather Station "P", Hawaii Ocean Time Series (HOT) and the southern Bering Sea.

In contrast to the open-ocean areas, the pCO_2 in waters from the southern Bering Sea decreased at a mean rate of -1.2 ± 1.2 $\mu atm\,y^{-1}$ (mean of three $10°\times10°$ boxes), which is estimated using additional data acquired since Takahashi et al. (2006). This estimate (that includes zero change) is subject to a large uncertainty that is caused by large seasonal amplitudes. Nevertheless, the negative trend may be attributed to the combined effects of increased biological production (Gregg et al., 2003) and/or changes in lateral and vertical mixing. The rates of change in $(pCO_2)_{sw}$ reported for the equatorial and North Pacific are summarized in Table 2. At the HOT site (28.8°N, 158°W), Dore et al. (2003) and Keeling et al. (2004) both reported a rate of $2.5\,\mu atm\,y^{-1}$ for 1988–2002, which is twice as fast as the 1974–2006 mean rate of $1.15\pm0.17\,\mu atm\,y^{-1}$ shown in Fig. 5B. As already discussed in Takahashi et al. (2006), the difference may be attributed to the periods represented and sampling frequencies.

The rate of change in the equatorial Pacific belt is complicated by the El Niño events and phase shifts in the Pacific Decadal Oscillation (PDO) as discussed by Feely et al. (2002), Takahashi et al. (2003) and Feely et al. (2006), and varies between −0.9 and $3.4\,\mu atm\,y^{-1}$ (see Table 2). The 1974–2005 mean for all the observations for the western and central equatorial Pacific is $1.3\pm0.6\,\mu atm\,y^{-1}$.

3.4. South Pacific Ocean

Six $5°\times10°$ areas located between 20° and 55°S have enough observations for the assessment of decadal change in surface water pCO_2. Fig. 6 shows the time trends observed in three representative areas in the South Pacific. Since the effects of El Niño (gray dots) are not discernible, the rates of change are computed using all data. The mean rates of change for surface water pCO_2 and SST for the six box areas (Table 3) give a mean rate of change of $1.5\pm0.3\,\mu atm\,y^{-1}$. The rates of change of SST estimated using the temperature data obtained concurrently with pCO_2 measurements are consistent with those based on the more extensive data set of Reynolds et al. (2003).

3.5. Subpolar Southern Ocean

The observations made in the Southern Ocean south of 50°S increased significantly not only in numbers from 0.4 M in the database used in Takahashi et al. (2002) to about 1.1 M in this database, but also in geographic coverage (Fig. 1A). On the other hand, based upon a global biogeochemical ocean general circulation model to simulate air–sea flux and sea–air pCO_2 differences over the Southern Ocean (south of 40°S), Lenton et al. (2006) proposed a sampling strategy. They estimated that sampling every 3 months along N–S traverses of 30° apart in longitude and at every 3° in latitude is necessary for obtaining the annual CO_2 uptake flux within ±0.1 Pg-C y^{-1} (or the mean annual sea–air pCO_2 difference of about $\pm2\,\mu atm$). As seen in Figs. 1A and B, our N–S traverses with more than 5 months of observations are clustered over five belts over the Southern Ocean and are on the average about 70° apart, which is farther apart than twice the desired intervals of 30°. However, our N–S sampling density appears to be sufficient. Therefore, the climatological mean values reported for the Southern Ocean are subject of errors from this level of undersampling.

Because of the strong zonal structure of the subpolar waters of the Southern Ocean, the surface water pCO_2 data in ice-free areas are examined for decadal changes according to the zonal distribution of SST. In this region the surface water pCO_2 undergoes large seasonal changes (~60 μatm) (Metzl et al., 1995, 1999, 2006) due to deep mixing in winter and photosynthesis in summer (Bakker et al., 1997; Hales and Takahashi, 2004). To minimize the large time–space variability caused by the

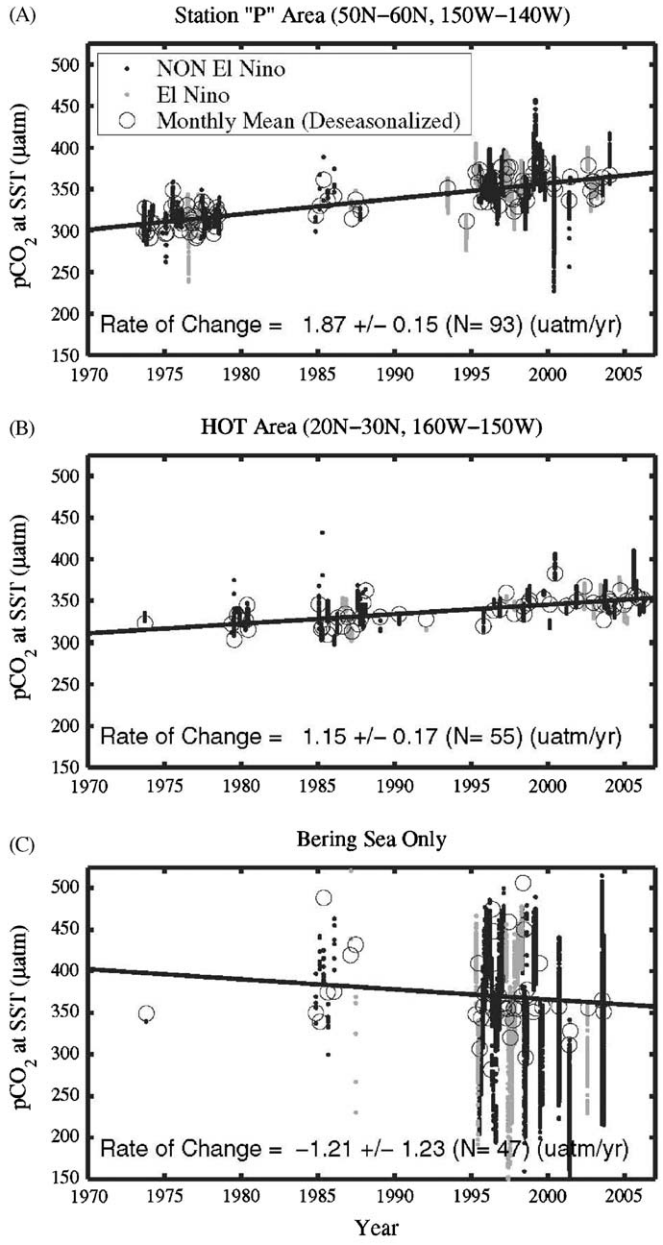

Fig. 5. Temporal change in the surface water pCO_2 (A) in the Station "P" area, (B) HOT area and (C) southern Bering Sea. These plots have been updated using the data obtained since Takahashi et al. (2006). Black dots indicate the observed values during non-El Niño periods, and gray dots those during El Niño periods. Open circles indicate the deseasonalized mean monthly values, and the solid line shows a linear regression computed using the mean monthly values. The mean rate of change is shown at the bottom of each panel. *N* is the number of monthly mean values used. The El Niño values are indistinguishable from the non-El Niño values.

photosynthetic drawdown of pCO_2, only the data obtained south of 50°S during the austral winter months (days of year from 172 to 326 between the two solstices) are analyzed in order to detect decadal change in the surface water pCO_2. The austral winter observations span the 20-year period from 1986 to 2006, and are from all around the continent (see Fig. 1A), although they are more frequent in the Kerguelen, Drake Passage and New Zealand-Ross Sea areas. The data are binned into six 1°C-wide circumpolar SST zones ranging from 0.8 to 6.5 °C, and the mean rate of pCO_2 change in each zone is computed by linearly regressing monthly mean values (Fig. 7 and Table 4). Since all data used were observed in the winter months in various years, deseasonalization corrections are not necessary. The data in three of the six SST zones are shown in Fig. 7. Although variability in ocean circulations and ice fields in the Southern Ocean are related to the El Niño/Southern Oscillation (ENSO) (e.g., Simmonds and Jacka, 1995; Yuan and Martinson, 2000), no discernible differences in ocean pCO_2 are observed for El Niño periods. An overall mean rate for the circumpolar sub-Antarctic surface waters is estimated to be $2.1 \pm 0.6\,\mu atm\,y^{-1}$. Three zones with temperatures between 1.5 and 4.5 °C, which straddle the Antarctic Convergence Zone, tend to have higher rates than the atmospheric increase rate of 1.5 µatm y^{-1}. We speculate that these high values may reflect an increase in vertical mixing rates of high-CO_2 subsurface waters.

3.6. Seasonal ice zone around Antarctica

An increasing number of pCO_2 observations have become available as a result of improved ice-field capabilities of research icebreakers. Twelve thousand observations made in ice-field waters (SST $\leqslant -1.75$ °C) south of about 60°S within seasonal ice fields during the austral winter months (June–September in various years) are summarized in Fig. 8, and show a steady increase from about 340 µatm in early June to about 410 µatm in the end of September, far exceeding the atmospheric pCO_2 of about 357 µatm. A similar trend has been observed during the winter months of 1993–1995 at the Prydz Bay station (68°34′S, 78°55′E) by Gibson and Trull (1999), although their pCO_2 values were systematically lower than ours by about 50 µatm. The difference may reflect the waters at their location, and/or may be attributed to their pCO_2 values that were calculated using TCO_2 and pH measurements.

These data in Fig. 8 represent the under-ice waters, which may be exposed to the air and exchange CO_2 through polynyas, leads and cracks in the ice fields. The increasing pCO_2 suggests that, as the winter season progresses, the water chemistry is increasingly affected by mixing with deeper waters and/or respiration within the under-ice mixed layer. This is consistent with the low oxygen concentrations observed in the ice-field waters of the Weddell Sea (Gordon et al., 1984), the Prydz Bay (Gibson and Trull, 1999) and the Ross Sea (Sweeney, 2003). Brine rejection during ice formation may also contribute some high CO_2 waters (Nomura et al., 2006). Therefore, the seasonal ice fields surrounding Antarctica are considered to be a potential source for atmospheric CO_2 as indicated by positive ΔpCO_2 observed by Bakker et al. (1997), Bakker et al. (2008) and Bellerby et al., (2004) in the Weddell gyre and by Rubin et al. (1998) in the Amundsen–Bellingshausen Seas shortly after the retreat of the ice. In contrast, Stoll et al. (1999) observed that the ice-field waters in the Weddell Sea had negative ΔpCO_2 (30 µatm below the atmospheric) in early winter of April–May 1996, and proposed that the Weddell Sea could be a significant CO_2 sink throughout the winter. The observations presented in Fig. 8 (i. e. $pCO_2 > 360$ µatm after June) as well as the work cited above do not support their extrapolation of the early winter observations into the peak winter months. We speculate that the observations of Stoll et al. (1999) may represent a remnant of the low pCO_2 water formed during earlier seasons (Sweeney et al., 2000; Sweeney, 2003; Hales and Takahashi, 2004; Metzl et al., 2006).

The data shown in Fig. 8, however, include observations made only along several N–S transects (65 ± 5°W, 170 ± 10°W, 20 ± 10°E, 90 ± 30°E and 120 ± 20°E) over a 10-year period, and, by no means reflect the time–space variability of pCO_2 in ice-field waters occurred during the decade. Nevertheless, because of the limited observations, we assume that the observed relationship applies universally for the ice-field waters around the continent, and estimate the pCO_2 in ice-field waters as a function of time of year

Table 2
Mean rates of change in surface water pCO_2 in the North and Equatorial Pacific.

Oceans	Locations ($\mu atm\,y^{-1}$)	Rates	Remarks & References
S. Bering & Okhotsk Seas	Subarctic marginal seas	-1.1 ± 0.6	1974–2002 mean of four $10^\circ\times10^\circ$ boxes; Takahashi et al. (2006)
S. Bering Sea	Bering Sea south of 58°N	-1.2 ± 1.2	1974–2004 mean of three $10^\circ\times10^\circ$ boxes; This study
N. Pacific Basin	Open N. Pacific North of 10°N	1.2 ± 0.5	1970–2004 mean of 28 $10^\circ\times10^\circ$ boxes; Takahashi et al. (2006)
Western	7–33°N	1.2 ± 0.9	1984–1993; Inoue et al. (1995)
North Pacific	137°E	1.6 ± 0.2	1983–2003; Midorikawa et al. (2005)
N. Central Pacific	28.8°N, 158°W	2.5 ± 0.3*	1989–2001; Dore et al. (2003)
HOT Time Series		2.5 ± 0.1*	1988–2002; Keeling et al. (2004)
Central Eq. Pacific	5°N–5°S	-0.9 ± 1.3	1979–1990, non-El Niño periods
Nino 3.4 area	120–170°W	1.3 ± 0.9	1990–2001, non-El Niño periods; the 1990 change may reflect a phase shift in Pacific Decadal Oscillation; Takahashi et al. (2003)
		1.7 ± 1.4	1985–1998, El Niño periods; Takahashi et al. (2003)
Central Eq. Pacific	5°N–5°S	1.1 ± 0.3	1974–2005; non-El Niño periods;
Nino 3.4 area	120–170°W	2.5 ± 0.9	1974–2005; El Niño periods; Feely et al., (2006)
Western Eq. Pacific	5°N–5°S	0.5 ± 0.3	1980–1990; non-El Niño periods;
Warm Water Pool	180°W–175°E	3.4 ± 0.4	1990–2001, non-El Niño periods; Takahashi et al. (2003)
Western Eq. Pacific	5°N–5°S	2.2 ± 0.3	1981–2005; non-El Niño periods;
Warm Water Pool	180°W–175°E	0.9 ± 0.4	1983–2003; El-Niño periods; Feely et al. (2006)
Eq. Pacific	10°N–5°S	2.0 ± 0.2	1990–2003; El Niño included;
Divergence Zone	95°W–150°E		$S\geqslant34.8$; Ishii et al. (2004)
Western Eq. Pacific	10°N–5°S	1.2 ± 0.1	1990–2003; El Niño included;
Warm Water Pool	160°W–135°E		$S<34.8$; Ishii et al. (2004)

The rates with * are estimated using the total alkalinity and TCO_2 data, and all other are based on direct measurements of pCO_2 in seawater. Uncertainties are defined by Eq. (5) in Section 3.1.

regardless of location, when observations are not available. Obviously, this approximation needs to be improved in the future as more observations are accumulated.

3.7. South Atlantic and Indian Oceans

As shown in Fig. 1, not enough pCO_2 measurements are available in the South Atlantic and Indian Oceans for estimating the multi-decadal mean rates.

3.8. Global summary

On the basis of the surface water pCO_2 data measured during the past three decades, the mean rate of increase in about 27% of the global ocean areas is estimated to be in a range of 1.26 (±0.55) to 2.13 (±0.64) $\mu atm\,y^{-1}$ (Table 5). Because of insufficient sampling, the rate for the Indian and South Atlantic Oceans as well as for large areas of the South Pacific cannot be assessed satisfactorily as yet. The mean rate for the North Atlantic ($1.80\pm0.37\,\mu atm\,y^{-1}$) appears to be somewhat higher than that for the North Pacific ($1.28\pm0.46\,\mu atm\,y^{-1}$), although they overlap within respective standard deviations. On the other hand, since the rate of change depends not only on the air–sea CO_2 flux but also on the lateral and vertical transport of waters, regional differences in the rate are expected. On the basis of the available database, the difference between these two ocean basins cannot be firmly established.

The area-weighted mean for the rates for the 78 box areas (27% of the ocean area including the Southern Ocean) determined in this study is $1.69\pm0.51\,\mu atm\,y^{-1}$, and that for 72 box areas (17% of the ocean area excluding the Southern Ocean) is $1.45\pm0.47\,\mu atm\,y^{-1}$ (Table 5). These two mean values are given since the rate for the Southern Ocean represents only for the winter months, whereas the rates for other ocean basins are for all seasons. In addition, as a result of various degrees of undersampling in time and space, including the assumed time-independent seasonal variability in each box area, the uncertainties for mean rates of surface water pCO_2 change are minimum estimates. Furthermore, the rates for the remaining 73% of the ocean areas are not available. Therefore, a global ocean mean rate of increase is taken to be $1.5\,\mu atm\,y^{-1}$, the mean of these two mean values. This rate is used throughout this study to normalize the pCO_2 data to a reference year 2000, with the exception of the Bering Sea where the observed rate of $-1.2\,\mu atm\,y^{-1}$ is used. In Section 6.3, the sensitivity of the sea–air CO_2 flux to various pCO_2 increase rate will be discussed. However, until the rates of pCO_2 increase in regional scales are more firmly established in the future, use of regionally specific increase rates is not justified.

The mean annual rate of atmospheric CO_2 increase fluctuated between about 0.8 and $2.9\,\mu atm\,y^{-1}$ (or $ppm\,y^{-1}$) in 1970–2006, whereas the corresponding annual changes for surface water pCO_2 cannot be computed reliably due to its large seasonal variation and small annual increases (Figs. 3, 5 and 6). Because of the differences between processes and time-scales regulating the atmospheric and oceanic pCO_2, the individual annual rates cannot be compared. On the three-decade average, however, the rate of oceanic pCO_2 increase, appears to be similar to that for the atmospheric pCO_2 increase. This suggests that the sea–air CO_2 exchange is a dominant process for regulating the surface water CO_2.

4. Method for time–space interpolation

Using the procedures explained in Section 3, all observations are corrected to the single reference year 2000. For the interpolation scheme used for this study, the pCO_2 values must be binned into 642,000 space–time pixels that represent a $4^\circ\times5^\circ$ computational grid for each day in the single reference year (= 1759 box areas × 365 days). In the northern and equatorial ocean areas north of 12°S, there are observations in many of these pixels (Fig. 1), and hence the daily mean value in each pixel is used. On the other hand, fewer observations are available in the Southern Hemisphere, and many pixels have no data. Since this makes our interpolation solutions unstable for the areas south of 12°S, available observations were propagated to neighboring pixels

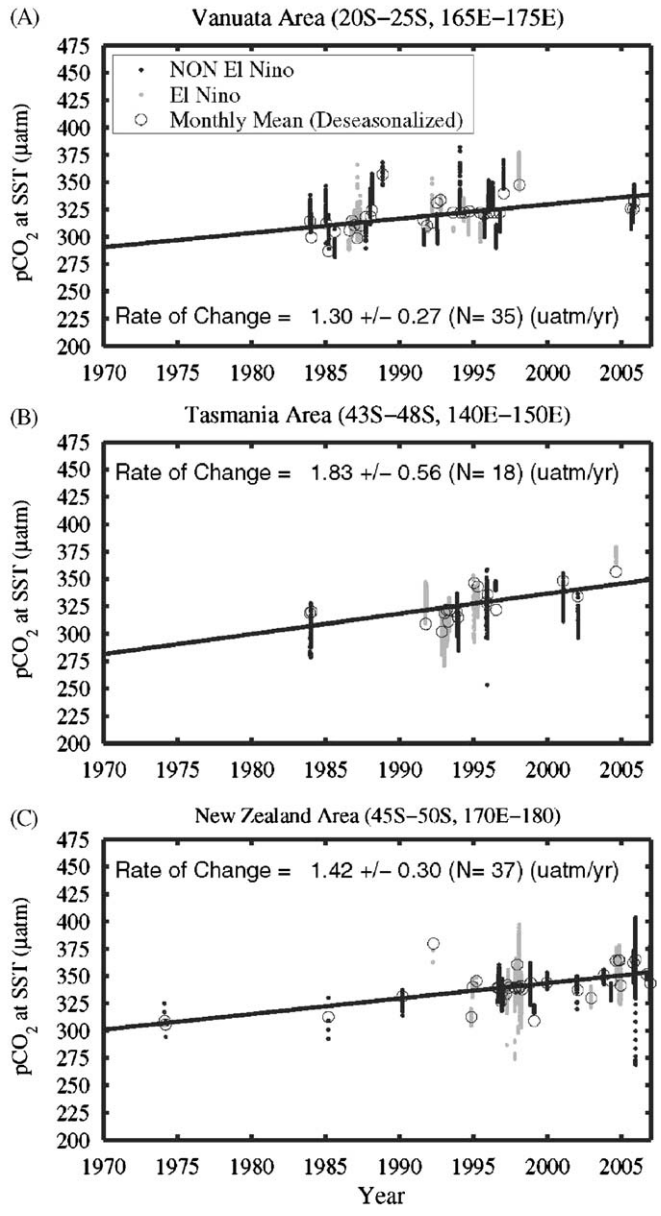

Fig. 6. Rates of increase in surface water pCO_2 in three areas in the temperate South Pacific: (A) Vanuata area, (B) Tasmania area and (C) New Zealand area. Solid dots (black for non-El Niño periods and gray for El Niño periods) indicate individual measurements, and open circles are the deseasonalized monthly mean values. The effects of El Niño events are not discernible. The mean annual rate of change is computed using a linear regression for the deseasonalized mean monthly values.

with no observations by including the values in neighboring areas for $\pm 4^\circ$ latitude, $\pm 5^\circ$ longitude and ± 1 day from the center of a pixel. The mean is computed by weighting a measured value inversely proportional to its time-space distance from the pixel center. This procedure is equivalent of increasing the size of pixels to four neighboring pixels over 3 days (past, present and future by 1 day). After the above procedures are applied, about 50% of the space–time pixels over the global oceans have measured values.

To estimate pCO_2 values in the boxes without observations, an interpolation equation based on 2-D diffusion–advection transport equation for surface waters is used:

$$dS/dt = K\nabla^2 S - (\partial S/\partial x\, Vx + \partial S/\partial y\, Vy) \quad (6)$$

where $\nabla^2 S = \partial^2 S/\partial x^2 + \partial^2 S/\partial y^2$.

S is a scaler quantity, K is lateral eddy diffusivity set at a canonical value of $2000\,m^2/s$ for surface waters (Thiele et al., 1986), and Vx and Vy are monthly mean advective velocities for surface waters. For the advective flow field, the monthly mean of Toggweiler et al. (1989) is used. This equation is discretized onto a 5° longitude by 4° latitude spatial grid over the globe, and solved iteratively using a finite difference algorithm (Takahashi et al., 1995, 1997). Material transport across the sea–land interface is assumed to be negligibly small: $\partial S/\partial x = 0$ and $\partial S/\partial y = 0$. Singularities at the poles are avoided by the presence of Antarctica in the south and by treating the Arctic ice field as land in the north. The surface water pCO_2 values are the solutions obtained after 500 iterations. This is determined on the basis of behaviors of the temperature values that are interpolated using the same method described above.

In this interpolation scheme, the observations are satisfied explicitly, and those in pixels that have no observations are computed by the continuity equation. The effects of internal sources and sinks of CO_2, exchange with atmosphere and upwelling of deep waters are considered imbedded in the observed data, and accordingly, terms for internal source and sink and exchange fluxes are neglected in Eq. (6). While the interpolation scheme yields daily values, the monthly mean values for each box area are presented in this paper.

5. Climatological mean distribution of surface water pCO_2

5.1. Global distribution

The climatological mean distribution of ΔpCO_2 in each month for the reference year 2000 (Fig. 9) is computed using the monthly mean surface water pCO_2 values over the global ocean and the mean monthly atmospheric pCO_2 values for the year 2000 as described in Section 2. It should be pointed out that any differences between the new and the previous maps for the reference years 1990 (Takahashi et al., 1997) and 1995 (Takahashi et al., 2002) do not indicate changes occurred in the oceans from 1990 to 2000, but rather reflect primarily the improved database as well as the improvements in the normalization method for the reference year as described in Section 3.

5.2. Regional distribution

To show the seasonal and regional changes in ΔpCO_2 more clearly, monthly mean ΔpCO_2 data are plotted in Fig. 10 for six climatic zones in the four ocean basins. The tropical belt ($14^\circ N$–$14^\circ S$) of the oceans has high positive values with little seasonal variability, indicating that the area is a strong source for CO_2 year around. The tropical Pacific (Fig. 10B) has the highest positive ΔpCO_2 values (annual mean of 27 µatm), the tropical Atlantic (Fig. 10A, annual mean of 18 µatm) next, and the tropical Indian (Fig. 10C, annual mean of 15 µatm) the lowest. The temperate Atlantic and Pacific (14–50° in the both hemispheres) exhibit large seasonal changes, positive ΔpCO_2 in warm summer months and negative values in colder winter months reflecting the dominant effect on $(pCO_2)_{sw}$ of seasonal SST changes. However, the peak-to-peak amplitude for the temperate North Atlantic is about 42 µatm, and is somewhat larger than 37 µatm for the temperate North Pacific. Since the mean seasonal amplitudes for SST are similar in these two ocean areas (5.7 and 5.8 °C), the difference in ΔpCO_2 amplitudes cannot be attributed to SST, and may reflect differences in biological environments such as a greater supply of nitrate by the nitrification of atmospheric nitrogen in the North Atlantic (Capone et al., 2005). Seasonal

Table 3
Mean rates of change in surface water pCO_2 and bulk water temperature of mixed layer (SST) estimated in six areas in the temperate South Pacific Ocean.

Locations	Lat.	Long.	Data period	Rate of change		No. of MOS.	Rate of change	
				pCO_2@SST ($\mu atm\,y^{-1}$)	$\pm\sigma$ ($\mu atm\,y^{-1}$)		SST ($^{\circ}C\,y^{-1}$)	$\pm\sigma$ ($^{\circ}C\,y^{-1}$)
Tahiti	15–20°S	135–145°W	11974–1997	2.00	0.39	16	0.033	0.034
Vanuata	20–25°S	165–175°E	1984–2006	1.30	0.27	35	−0.048	0.018
New Caledonia	25–30°S	170–180°W	1974–2005	1.05	0.09	17	−0.033	0.020
Tasmania	43–48°S	140–150°E	1984–2004	1.83	0.56	18	−0.051	0.062
New Zealand	45–50°S	170–180°E	1974–2006	1.42	0.30	37	0.001	0.027
S. of Tasmania	50–55°S	140–150°E	1984–2002	1.61	0.20	12	−0.044	0.064
Mean				1.5 ± 0.3	0.30	–	−0.02 ± 0.05	0.04

The rates are computed using mean monthly values. The temperatures are measured concurrently with pCO_2.

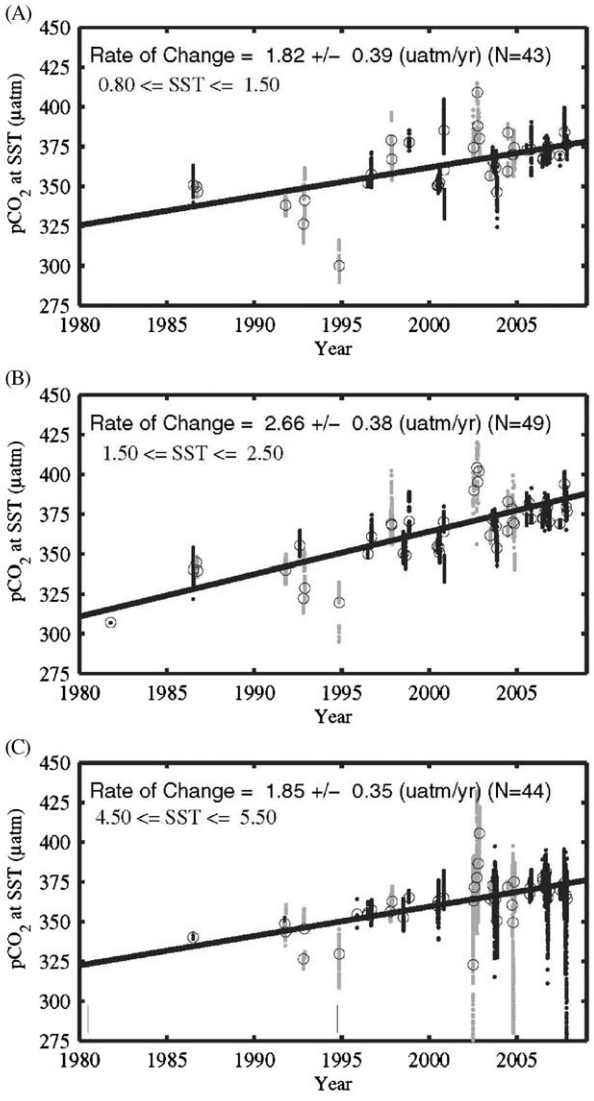

Fig. 7. Rates of increase in surface water pCO_2 in the subpolar region (south of 50°S) of the Southern Ocean in the austral winter months (day of year from 172 to 326) during the period from 1986 to 2007: (A) SST between 0.80 and 1.50 °C, (B) SST between 1.50 and 2.50 °C, and (C) SST between 4.50 and 5.50 °C. Black dots indicate measurements made in non-El Niño periods; and gray dots indicate those made in El Niño periods. No discernible differences are seen between these periods. The mean rates are estimated by linearly regressing the monthly mean values (open circles); and *N* is the number of monthly mean values.

Table 4
Mean rate of increase for pCO_2 in winter-time surface waters (Year dates 172–326) in various SST bands over the subpolar Southern Oceans for the period 1986–2007.

Temperature range (°C)	Rate of pCO_2 Change ($\mu atm\,y^{-1}$)	No. months (*N*)	Data counts
0.80–1.50	1.82 ± 0.39	43	3915
1.50–2.50	2.66 ± 0.38	49	7733
2.50–3.50	2.80 ± 0.39	43	8084
3.50–4.50	2.61 ± 0.58	43	13,968
4.50–5.50	1.85 ± 0.35	44	15,463
5.50–6.50	1.18 ± 0.40	42	17,077
0.80–6.50	Mean 2.1 ± 0.6	264	66,240

The rates are estimated by a linear regression of monthly mean values made during the winter months within each SST band. *N* is the number of months used for the regression, and ± uncertainties are computed using Eq. (5). The area-weighted mean rate for the circumpolar zone is 2.1 ± 0.6 $\mu atm\,y^{-1}$, where ± ⊖ uncertainty is one standard deviation of the six zonal mean values.

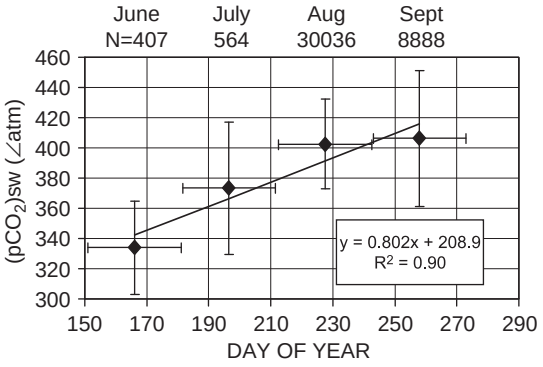

Fig. 8. Multi-year pCO_2 data observed in ice field waters with temperatures less than −1.75 °C in the Southern Ocean south of 60°S during the austral winter months, June–September. The pCO_2 increases with progressing seasons. The values are not corrected for the reference year; and *N* indicates the number of pCO_2 measurements. When these waters are exposed to the air, they are a source for CO_2 since they have pCO_2 values greater than those in the overlying atmosphere by as much as 40 ± 20 µatm during the late winter months (August–September).

changes in the northern temperate oceans are about 6 months out of phase from the southern temperate oceans.

The annual mean ΔpCO_2 for the southern temperate Atlantic (−10 µatm, 14–50°S) is similar to that for the southern Pacific of −10 µatm, while the southern temperate Indian has more negative ΔpCO_2 values with a mean of −17 µatm (Fig. 10C). The regional mean SST for the temperate South Indian (18.6 °C) is

Table 5
Summary of mean rates of increase in surface water pCO_2.

	No. of box areas	Ocean area[a] (10^6 km^2)	Annual[b] rate (μatm y^{-1})	Standard deviation (μatm y^{-1})	References
N. Pacific (10–60°N)[c]	28	28.9	1.28	0.46	Takahashi et al. (2006)
Equatorial Pacific (5–5°S)[d]	2	7.4	1.26	0.55	Feely et al. (2006)
N. Atlantic (15–70°N)[e]	36	16.8	1.80	0.37	This study
S. Pacific (15–55°S)[e]	6	2.9	1.53	0.35	This study
Southern O. (50–60°S)[f]	6	30.6	2.13	0.64	This study
Global with Southern Ocean	78	86.6 (27%)	1.69	0.51	
Global without Southern Ocean	72	56.0 (17%)	1.45	0.47	

While the rate for the Southern Ocean is estimated for the winter months only, all other rates represent seasonal mean.
[a] Global ocean area = 326.5×10^6 km^2.
[b] Area-weighted mean.
[c] 10°(lat.) × 10° (long) boxes, excluding the Bering Sea.
[d] Nino 3.4 (120–170°W) and Western Warm Pool (165–175°E) areas.
[e] 5°(lat.) × 10°(long.) boxes.
[f] Winter data only for circumpolar 2° (lat.) wide bands.

similar to that for the South Pacific (18.9 °C) and somewhat higher than the South Atlantic (17.4 °C), and the mean annual surface water salinity values are also similar (35.0 for the South Indian, 35.4 for the South Atlantic and 35.1 for the South Pacific). Hence, the low pCO_2 in the South Indian Ocean cannot be attributed to differences in SST or salinity. Primary productions estimated from the SeaWiFS observations (Gregg et al., 2003) suggest that the mean annual productivity in the South Indian is higher than in the South Pacific, but lower than the South Atlantic. Hence, the biological production data cannot account for the ΔpCO_2 data. It is possible that the ΔpCO_2 data and hence the fluxes could be biased because of undersampling in the Southern Hemisphere oceans (see Fig. 1).

A strong negative ΔpCO_2 observed in the spring–summer months in the sub-arctic Atlantic (Körtzinger et al., 2008) and Pacific (Fig. 10A and B) are due to the effect of biological drawdown of CO_2, in strongly stratified shallow mixed layers. The seasonal ΔpCO_2 change in subpolar regions is about 4 months out of phase from that for the adjacent temperate region.

The positive ΔpCO_2 values observed in July–September in the northern Indian Ocean (north of 14°N, Fig. 10C) is due to the seasonal upwelling of deep waters caused by the Southwest Monsoon winds. The positive peak observed in July–October in the seasonal ice zone of the Southern Ocean (south of 62°S, Fig. 10D) represents the under-ice mixed water layer that is enriched with CO_2 and nutrients primarily by the vertical mixing of deep waters. During the austral spring–summer months, phytoplankton blooms occurring near ice margins and within polynyas reduce ΔpCO_2 values as low as −100 µatm. However, extent and duration of bloom areas that form a strong sink for atmospheric CO_2 may vary geographically and have not been well documented.

5.3. Comparison with the 2002 results

Takahashi et al. (2002) used the following procedures for correcting the pCO_2 data to a reference year 1995. They considered that the surface water values in tropical and temperate oceans (45°N–50°S in the Atlantic, north of 50°S in the Indian Ocean and 40°N–50°S in the western Pacific west of the date line and 40°N–60°S in the eastern Pacific east of the date line) were increasing at the same rate as the atmospheric pCO_2. As done for this study, they corrected the observed values to the reference year using a mean atmospheric CO_2 increase rate of 1.5 µatm. On the other hand, on the basis of a limited number of the pCO_2 observations in high latitudes, they considered that CO_2 properties in surface waters in subpolar and polar regions remained unchanged year to year due to the dilution by vertical mixing of deep waters that were little affected by the atmospheric CO_2 increase. Accordingly, they made no correction for the time of pCO_2 observations. In contrast, we have demonstrated in this study that the surface water pCO_2 over the subpolar oceans has been also increasing at a mean rate of 1.5 µatm y^{-1} (ranging between 1.3 and 2.0, see Table 5), and used this mean rate for normalizing the multi-year data to a reference year of 2000 for the entire oceanic areas with the exception of the Bering Sea, where the observed rate of −1.2 µatm y^{-1} is used.

The difference maps between the surface water pCO_2 values from this study (3.0 M) and the 2002 study (0.94 M) are shown in Fig. 11: (A) February and (B) August. To make these two studies comparable, the 2002 values, which were normalized to a reference year 1995, are corrected by adding 7.5 µatm (= 1.5 µatm y^{-1} × 5 y) to adjust them to the reference year 2000. Reflecting the assumptions made in the 2002 study, larger differences are found in the subpolar to polar regions. Differences in the temperate and tropical areas are less than 5 µatm on the average. In the seasonal ice zone of the Southern Ocean south of about 62°S, the results of this study are found as much as 100 µatm greater than those of 2002 (Fig. 11B). This is attributed to the high pCO_2 values revealed by new measurements for under-ice waters during austral winter (Fig. 8). In the Arctic Chukchi Sea, the values for this study are found to be lower than those for the 2002 study by as much as 100 µatm both in February and August. Although this is attributed to new measurements, the time–space coverage of the Arctic waters is highly limited presently.

6. Net sea–air CO_2 flux

6.1. Computational method

The net sea–air CO_2 flux (F) is estimated using

$$F = k\alpha\Delta pCO_2 = Tr\Delta pCO_2 \quad (7)$$

where k is the CO_2 gas transfer velocity; α is the solubility of CO_2 in seawater; Tr is the sea–air gas transfer coefficient; and ΔpCO_2 is the sea–air pCO_2 difference in the reference year 2000 as defined by Eq. (4). The gas transfer velocity (k) is typically expressed as a power function of wind speed (U): $k \propto U^n$ at a given temperature and salinity. The value of exponent, n, has been suggested to be between 1 (Liss and Merlivat, 1986) and 3 (Wanninkhof and McGillis, 1999). Ho et al. (2006), on the basis of the $^3He/SF_6$ double tracer data obtained over high wind speed conditions (up to

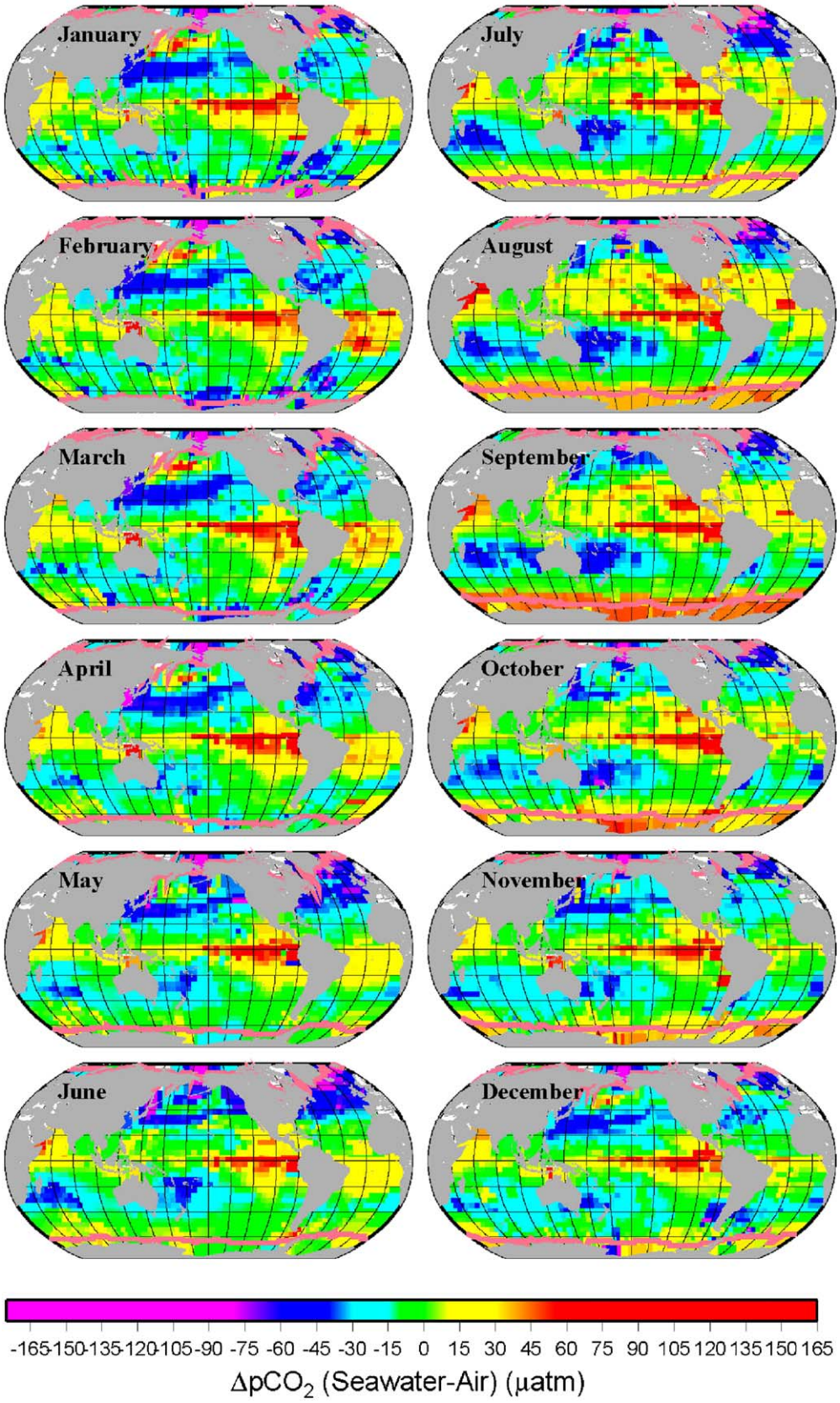

Fig. 9. The monthly mean values for sea–air pCO_2 differences in the global ocean. The values represent climatological mean for non-El Niño conditions adjusted to a reference year 2000. Orange–yellow colors indicate positive ΔpCO_2 (sea is a source for atmospheric CO_2), green indicates near zero ΔpCO_2, and cyan–blue colors indicate negative ΔpCO_2 (sea is a CO_2 sink). Heavy pink curves indicate the mean position for the northerly extent of 90% ice cover. Waters under the Southern Ocean ice-field have high positive ΔpCO_2. Whenever measurements are lacking for ice field waters, the values are estimated using the equation in Fig. 8. (For interpretation of the references to color in this figure legend, the reader is referred to the web version of this article.).

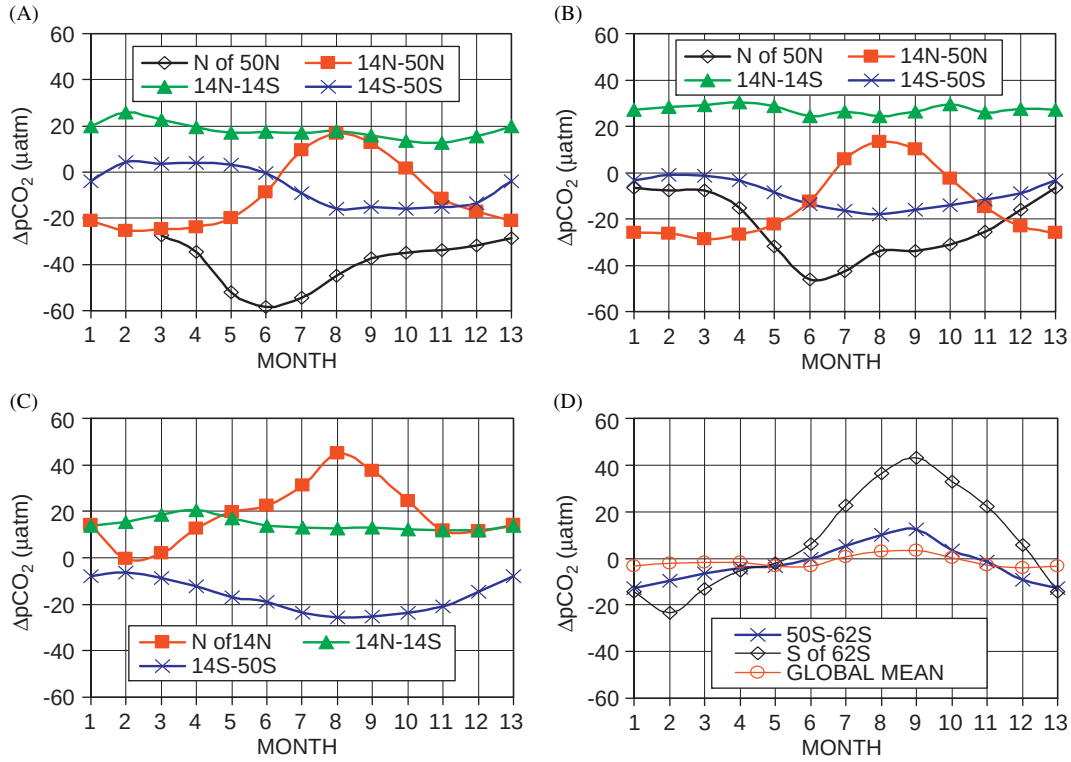

Fig. 10. The monthly mean values for sea-air pCO_2 differences in the four major ocean basins: (A) Atlantic, (B) Pacific, (C) Indian, (D) Southern and Global Oceans. Average values in each climatic zone are plotted against month (1 = January, 2 = February, …, 12 = December and 13 = January). The zones "50S–62S" and "S of 62S" in the Southern Ocean represent, respectively the open water zone and the seasonal ice zone.

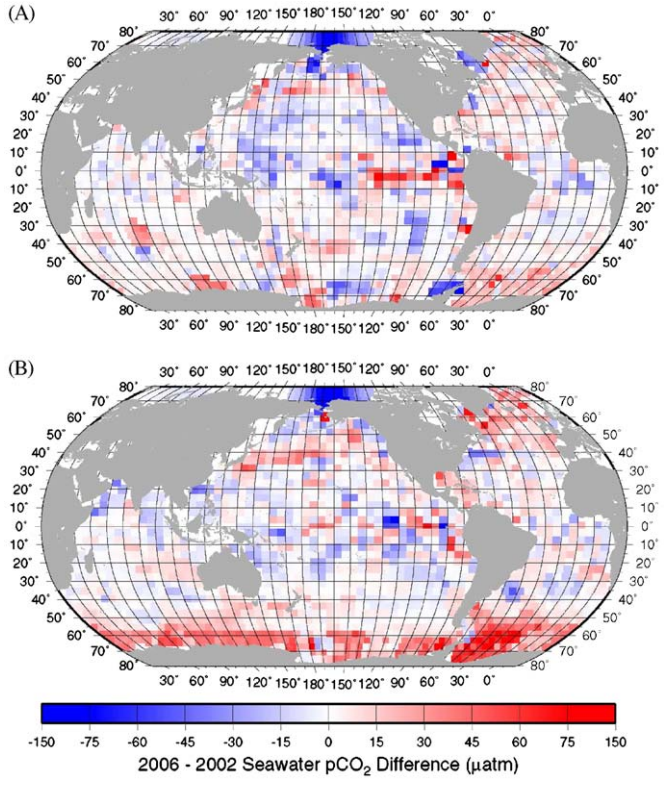

Fig. 11. Difference maps for the surface water pCO_2 values for this study and Takahashi et al. (2002): (A) February and (B) August. In order to make the results of these two studies comparable, the 2002 values, which were normalized to a reference year 1995, are corrected by adding 7.5 μatm ($= 1.5\,\mu atm\,y^{-1} \times 5\,y$) to adjust to the reference year 2000 used for this study.

$16\,m\,s^{-1}$) in the Southern Ocean, suggested a square dependence of wind speed. Considering various studies including Wanninkhof (1992), Nightingale et al. (2000) and Wanninkhof et al. (2004), we choose a formulation: $k\ (cm\,h^{-1}) = \Gamma\ (U_{10})^2\ (Sc/660)^{-1/2}$, where U_{10} is wind speed at 10 m above sea surface, and Sc is Schmidt number [= (kinematic viscosity of water)/(diffusion coefficient of CO_2 in water]. The value for a scaling factor, Γ, is evaluated according to the following procedures.

Wanninkhof (1992) used $^{14}CO_2$ as a diagnostic for sea–air CO_2 gas transfer, and estimated the scaling factor, Γ, of 0.39 based on a mean global wind speed of $7.4\,m\,s^{-1}$, and a mean gas invasion rate of $21\,cm\,h^{-1}$ derived from a simple box model to fit the global ocean bomb-^{14}C inventory of 2.89×10^{28} atoms that was estimated by Broecker et al. (1985). In our previous publication (Takahashi et al., 2002), this value for Γ was used. Improvements in the wind speed and ^{14}C data have resulted in smaller values for Γ as reviewed by Wanninkhof (2007). Naegler et al. (2006) pointed out that Γ depends on the ^{14}C inventory and wind speed field used, and that it must be evaluated for the same wind speed data used for the CO_2 flux calculations. Sweeney et al. (2007) have further extended this approach and inverted bomb-^{14}C data for ocean waters using three Ocean General Circulation Models, in which the global oceans are divided into 29 discrete surface areas. By their method, the time-space distribution of ^{14}C in surface waters, hence the gas transfer rates, is taken into account. To simplify computations, they assumed that the flux into each of the 29 areas has a time history proportional to the observed ^{14}C values in the atmosphere. Assuming a quadratic dependence of piston velocity on wind speed, they obtained a Γ value of 0.27 (for long-time average) using the 1954–2000 NCEP Reanalysis-I wind speeds (Kalnay et al., 1996) over the ice-free global oceans and the bomb-^{14}C inventory of $3.43 \pm 0.40 \times 10^{28}$ ^{14}C atoms as of 1994. This formulation yields not only piston velocity values consistent

with those obtained from some small-scale deliberate tracer studies (e.g. Nightingale et al., 2000), but also with the total bomb-^{14}C inventory obtained for the strato- and troposphere.

For this study, a Γ value of 0.26 has been computed using the 1979–2005 NCEP-DOE AMIP-II Reanalysis 6-h wind speed data (Kanamitsu et al., 2002), which is recast onto the same $4^\circ \times 5^\circ$ grid as used for this study. The value includes the effect of dilution of ocean water $^{14}CO_2$ by the uptake of fossil fuel CO_2 (free of ^{14}C). The wind speed data have a mean speed $\langle U_{10} \rangle$ of 8.06 m s^{-1} and $\langle U_{10}^2 \rangle / \langle U_{10} \rangle^2$ of 1.20 for ice-free oceans using the 6-h wind to calculate $\langle U_{10}^2 \rangle$. The overall error in Γ is estimated to be $\pm 30\%$ that includes uncertainties in the ^{14}C inventory, ocean models and $p^{14}CO_2$ (Sweeney et al., 2007).

6.2. Distribution of the sea–air CO_2 gas transfer coefficient

The product of the first two terms in Eq. (7) represents a sea–air CO_2 gas transfer rate constant (hereafter called gas transfer coefficient). When monthly mean wind speeds (U_{10} in the unit of meters s^{-1}) and α in (mol liter^{-1} atm^{-1}) (Weiss, 1974) are used, Eq. (8) gives the transfer coefficient (Tr):

$$\mathrm{Tr}(\mathrm{g-C\,m^{-2}\,month^{-1}\,\mu atm^{-1}}) = 0.585 \cdot \alpha \cdot (\mathrm{Sc})^{-1/2} \cdot (U_{10})^2 \qquad (8)$$

where 0.585 is a unit conversion factor taking into account the scaling factor for the gas transfer rate (0.26), (mol liter^{-1} atm^{-1}) to (g-C m^{-3} μatm^{-1}), (cm h^{-1}) to (m month^{-1}) ($= 10^{-2} \times 24 \times 365/12$), and a reference Schmidt number ($660^{1/2}$). The Schmidt number (Sc) and the solubility of CO_2 in seawater depend sensitively on the temperature: from 0° to 30 °C, Sc for CO_2 decreases by a factor of 5 and α also decreases by a factor of 2.5. Accordingly, the product $\alpha \cdot (\mathrm{Sc})^{-1/2}$ is nearly constant and changes by less than 10% over the temperature range of global surface ocean waters. Hence, the transfer rate coefficient, Tr, is primarily a function of wind speed. Since a product of Tr with ΔpCO_2 gives the net sea–air CO_2 flux, the seasonal and geographical variation of Tr is of interest.

In Fig. 12, the monthly mean Tr values in six climatic zones are summarized for the four major ocean basins and the global ocean. The subpolar regions of the North Atlantic (Fig. 12A, north of 50°N) and the Southern Ocean (Fig. 12D, 50–2°S) have the highest values for the transfer rate coefficient reaching as high as 0.12 g-C m^{-2} month^{-1} μatm^{-1} (hereafter the unit is omitted) due to persistent high winds during the regions' respective winter months. During the summer months, however, the Tr values decrease to as low as 0.03 in the sub-arctic Atlantic (Fig. 12A) and to 0.08 in the Southern Ocean (Fig. 12D). In contrast, winter-maximum Tr values reach only to 0.09 in the sub-arctic Pacific. The Antarctic zone (south of 62°S, Fig. 12D) has much lower wind speeds and hence shows lower Tr values ranging between 0.07 in winter and 0.05 in summer. In the temperate zones of the Atlantic and Pacific, the Tr values vary from summer values of about 0.03 to winter values of 0.07 (Fig. 12A and B); and the seasonal changes in the northern oceans are 6 months out of phase from the Southern Hemisphere oceans. The tropical Atlantic and Pacific (Fig. 12A and B, 14°N–14°S) have Tr values of about 0.03, and show very small seasonal variability. The northern Indian Ocean is significantly different from the Atlantic and Pacific. Tr values peak in June–August due to southwest monsoon winds in the tropical

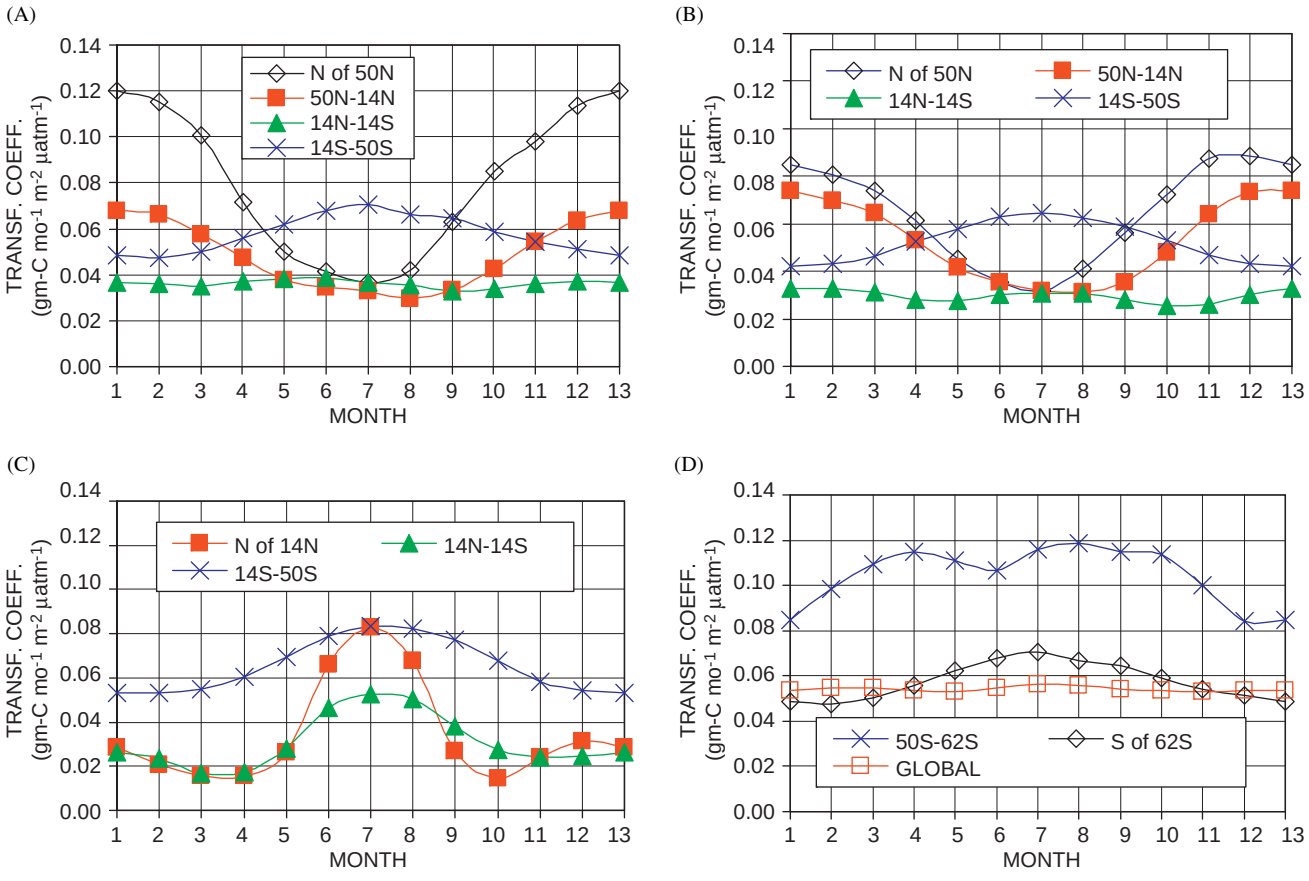

Fig. 12. Monthly mean values for the CO_2 gas transfer rate coefficient, Tr, in (g-carbon m^{-2} month^{-1} μatm^{-1}) computed using Eq. (8). The monthly mean values for U_{10} in each $4^\circ \times 5^\circ$ box were computed using the 1979–2005 NCEP-DOE AMIP-II Reanalysis data (updated version of Kanamitsu et al., 2002). The monthly mean values for each zone shown in the plots are area-weighted mean values of the box areas within each zone. Months are expressed as 1 = January, 2 = February,…, 12 = December and 13 = January.

zone and especially in the zone north of 14°N (Fig. 12C). The high wind speeds induce not only intense upwelling in the western Arabian Sea, but also cause high rates of sea–air gas exchange. The southern temperate Indian Ocean also has higher wind speeds than the southern Pacific and Atlantic, and hence higher Tr values ranging between 0.05 in summer and 0.08 in winter. The mean monthly values (area weighted) for the global ocean are nearly constant around 0.05 g-C month^{-1} m^{-2} μatm^{-1} (Fig. 12D).

6.3. Global distribution of the net sea–air CO_2 flux

The climatological mean sea–air CO_2 flux in each box area for each month is computed by multiplying monthly mean values for Tr (Eq. (8)) and ΔpCO2 (Eq. (4)) in each box. Since no significant correlation of individual ΔpCO_2 values with 6-h mean wind speed data is found in a single month, the product of monthly mean values is considered as a valid approximation for the CO_2 flux. Over the polar regions, where sea-ice fields form seasonally, the following assumptions are made for computing the sea–air CO_2 flux. When the ice cover is less than 10%, a box area is assumed to be all water. For ice covers between 10% and 90%, the flux is assumed to be proportional to open water area. Since ice fields have leads and polynyas due to dynamic motions of sea ice as evidenced by "sea smoke", we accept the estimates by Saunders and Ackley (personal communication) that 10% of fields is open water at any given time even in areas where satellite observations indicate 100% ice cover. The ice cover values used in this study are based on the NCEP/DOE 2 Reanalysis data (2005) (provided by the NOAA/OAR/ESRL PSD). The original data given in a Gaussian grid for 1970–2005 are re-gridded to our 4° × 5° grid, and the ice cover values in each pixel are averaged for each month (30.5 days).

6.3.1. Mean annual distribution

Fig. 13 shows the climatological mean annual sea–air CO_2 flux (g-C m^{-2} y^{-1}) for the reference year 2000, and Fig. 14 shows 4° zonal aggregates for the flux in the major ocean basins and the global oceans. The annual fluxes in six climatic zones in each ocean basin are summarized in Table 6. The equatorial Pacific is the most prominent source area for atmospheric CO_2 with a seasonally persistent sea-to-air flux of 0.48 Pg-C y^{-1}. Together with the tropical Atlantic and Indian Oceans, the global tropical oceans emit 0.69 Pg-C y^{-1} to the atmosphere. A belt of CO_2 sink zone is located in 20–50° latitudes in the both hemispheres (Fig. 14). This is attributed primarily to strong winds between 40° and 50°S, and the low pCO_2 values produced along the subtropical convergence zone, where the cooled subtropical gyre waters with low pCO_2 meet the subpolar waters with biologically-lowered pCO_2. Together, the mid-high latitude northern (22–50°N) and southern (22–50°S) oceans constitute, respectively a sink of −0.70 and −1.05 Pg-C y^{-1}. A sink area (−0.27 Pg-C y^{-1}) is seen also in the North Atlantic north of 50°N, including the Nordic Seas and portion of the Arctic. This is attributed to strong phytoplankton blooms in spring and strong cooling in winter. The annual CO_2 flux over the Southern Ocean seasonal ice zone is small due to the ice cover that reduces sea–air gas transfer in winter and by the cancellation of the seasonal source and sink fluxes.

The mean annual sea–air CO_2 flux values for the four major ocean basins are compared in Table 6. While the Atlantic has only 23% of the global ocean area, it takes up 41% of the annual global ocean flux of −1.42 Pg-C y^{-1}. On the other hand, while the Pacific has the largest area (47%), twice as large as the Atlantic, it takes up only 33% of the global flux. This is due to the large CO_2 source

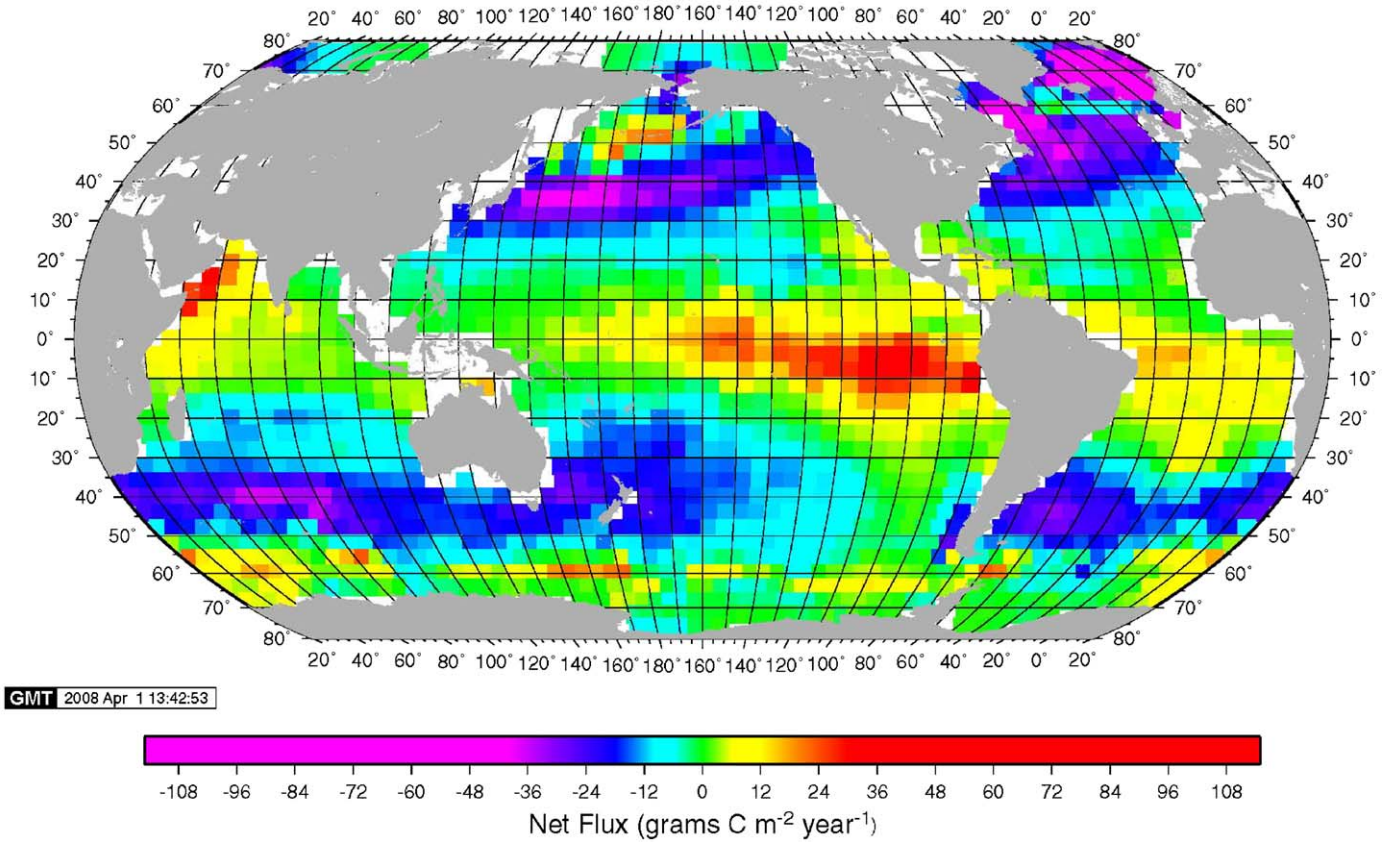

Fig. 13. Climatological mean annual sea–air CO_2 flux (g-C m^{-2} yr^{-1}) for the reference year 2000 (non-El Niño conditions). The map is based on 3.0 million surface water pCO_2 measurements obtained since 1970. Wind speed data from the 1979–2005 NCEP-DOE AMIP-II Reanalysis (R-2) and the gas transfer coefficient with a scaling factor of 0.26 (Eq. (8)) are used. This yields a net global air-to-sea flux of 1.42 Pg-C y^{-1}.

(+0.48 Pg-C y^{-1}) located along the equatorial Pacific. Since this source is reduced significantly due the El Niño events (Feely et al., 2006), the net uptake by the Pacific would be increased during these periods. The sink over the Southern Ocean is small due mainly to large seasonal ice cover that reduces gas exchange rates.

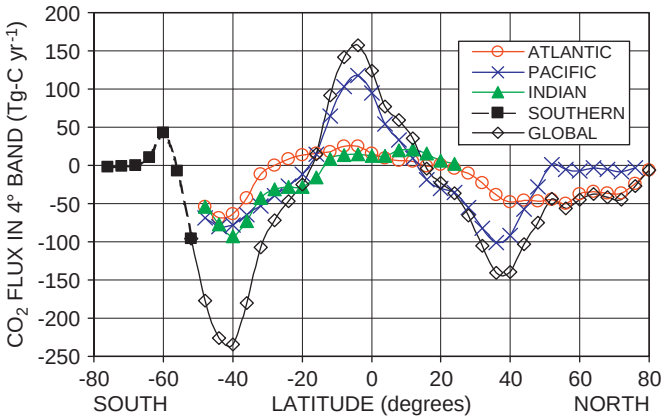

Fig. 14. Zonal mean sea–air CO_2 flux in the four major ocean basins. The flux values are expressed in Tg-C y^{-1} (Tg = 10^{12} g) for each 4°-wide zonal band across each ocean basin. This plot gives a total global air-to-sea flux of 1.42 Pg-C y^{-1}. The wind speed data are from the 1979–2005 NCEP-DOE AMIP-II Reanalysis, and the gas transfer coefficient is computed using Eq. (8).

The climatological mean value for the net air-to-sea flux for the reference year 2000 is estimated to be −1.42 Pg-C y^{-1} for the global oceans (Table 6). Errors for these estimates are discussed in Section 6.4.

6.3.2. *Seasonal variation of the global ocean sea–air CO_2 flux*

Fig. 15 shows the distribution of monthly mean flux in February and August in a reference year 2000. Seasonal changes in the flux field are clearly seen in the figures, and they are attributed to a combination of the effects of seasonal changes in water temperatures, biological utilization of CO_2 and water mixing as well as changes in wind speeds (Takahashi et al., 2002). The mid-latitude regions of the Atlantic, Indian and Pacific Oceans all change from a near-zero or weak source in the respective summer seasons to a strong sink in the respective winter seasons. This is due to the winter cooling of waters transported poleward by eastern boundary currents. In spring and summer, biological drawdown of CO_2 is to some extent offset by increase in pCO_2 due to warming. Subtropical gyres move from weak sinks in the winter seasons to weak sources in the summer seasons, consistent with the seasonal SST cycles, confirming the dominance of heating and cooling effects in controlling the seasonal variability in the pCO_2 and sea–air fluxes. At tropical latitudes, seasonality is most evident in the northwestern Indian Ocean, where the summer monsoon winds force upwelling of CO_2-rich subsurface waters coincident with high gas transfer rate (Tr) (Chen et al., 1998; Takahashi et al., 2002). The equatorial Pacific and Atlantic show little seasonal variability in CO_2 flux (Feely et al., 2002).

Table 6
Mean annual sea–air CO_2 fluxes (Pg-C y^{-1}) in the four major ocean basins and the global oceans for the reference year 2000 based on the 3.0 million pCO_2 measurements, the wind speed data from the 1979–2005 NCEP-DOE AMIP-II Reanalysis (rows marked 3.0 M and values in bold letters).

Zones	Areas 10^6 km^2	Data (M)	Sea-air CO_2 flux (Pg-C y^{-1})				
			Atlantic Ocean	Pacific Ocean	Indian Ocean	Southern Ocean	Zone sum
N of 50°N	16.2	**3.0**	**−0.27**	**−0.03**	–	–	**−0.30**
		0.94	−0.31	+0.01	–	–	−0.30
50–14°N	69.1	**3.0**	**−0.22**	**−0.50**	**+0.02**	–	**−0.70**
		0.94	−0.25	−0.47	+0.04	–	−0.68
14°N–14°S	86.7	3.0	**+0.10**	**+0.48**	**+0.10**	–	**+0.69**
		0.94	+0.11	+0.52	+0.13	–	+0.76
14–50°S	109.6	**3.0**	**−0.20**	**−0.41**	**−0.44**		**−1.05**
		0.94	−0.23	−0.37	−0.46	–	−1.06
50–62°S	29.7	3.0	–	–	–	**−0.06**	**−0.06**
		0.94	–	–	–	−0.34	−0.34
S of 62°S	15.3	3.0	–	–	–	**+0.01**	**+0.01**
		0.94	–	–	–	−0.04	−0.04
Basin/global		**3.0**	**−0.58**	**−0.46**	**−0.32**	**−0.05**	**−1.42**
% of flux		**3.0**	**41%**	**32%**	**23%**	**4%**	**100%**
		0.94	−0.66	−0.31	−0.29	−0.39	−1.65
		0.94	−40%	19%	18%	24%	100%
Area (10^6 km^2)	326.5		74.8	153.8	53.0	44.9	
% of area	100.0		23	47	16	14	

The gas transfer coefficient is computed using Eq. (8). The + values indicate sea-to-air fluxes; and the − values air-to-sea fluxes. The results for this study are compared with those for the reference year 1995 based on the 0.94 million measurements (marked 0.94 M with light letters) used by Takahashi et al. (2002). These fluxes are recomputed using the same wind speed data and gas transfer coefficients as used for this study. Hence the differences between these sets of flux values reflect the differences in the sea–air pCO_2 difference discussed in Section 5.3. The sink flux for the open Southern Ocean waters, 50–62°S, estimated by this study (3.0 M) is significantly smaller than that estimated on the basis of the earlier database of 0.94 M. This is attributed primarily to the improved database.

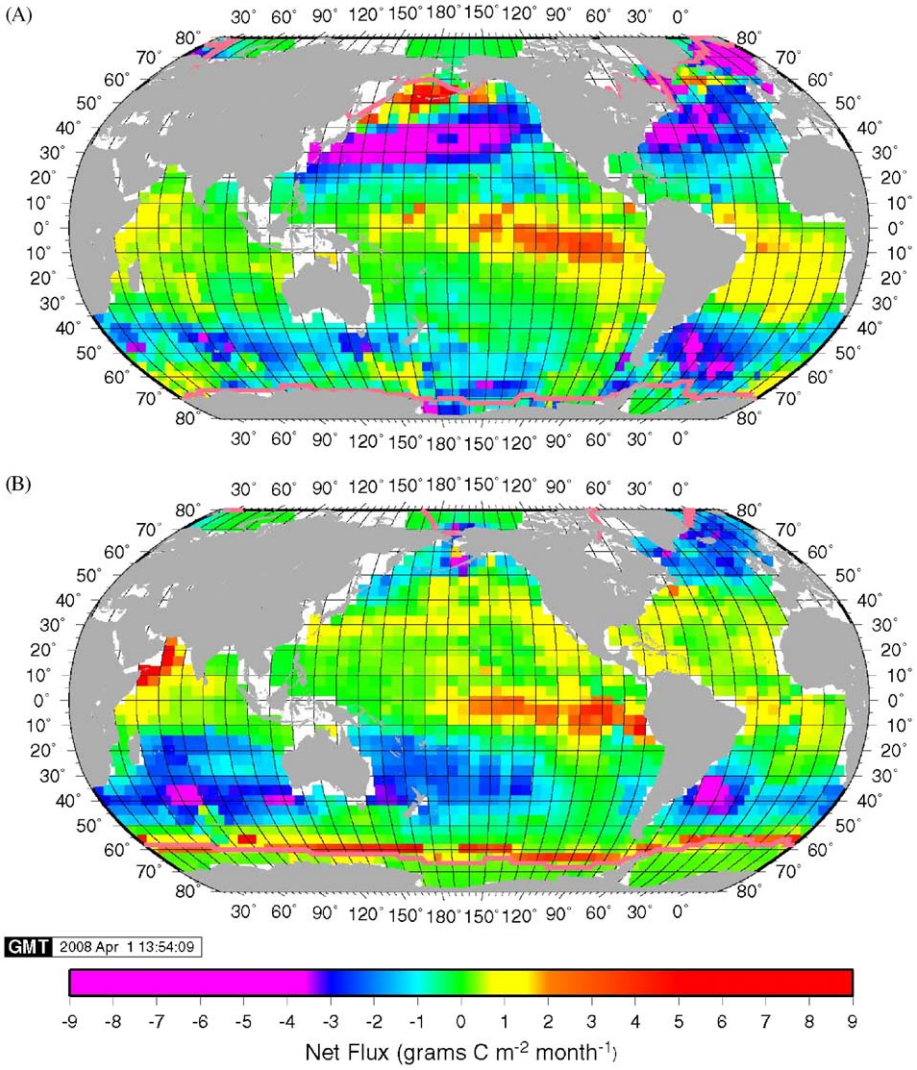

Fig. 15. Climatological mean sea–air CO_2 flux (g-C m^{-2} $month^{-1}$) in February (A) and August (B) in the reference year 2000. The wind speed data are from the 1979–2005 NCEP-DOE AMIP-II Reanalysis, and the gas transfer coefficient is computed using Eq. (8). Positive values (yellow–orange–red) indicate sea-to-air fluxes, and negative values (blue–magenta) indicate air-to-sea fluxes. Ice field data are from NCEP/DOE 2 Reanalysis (2005). (For interpretation of the references to color in this figure legend, the reader is referred to the web version of this article.).

Another striking seasonal feature is the band of moderate source waters (yellow–orange) located along the northern margins for the Antarctic sea-ice field in the vicinity of 60°S in August. This represents release of CO_2 from the high pCO_2 under-ice waters (see Fig. 8) along the ice-field edges. In the areas southward of the edge lines, the open water areas are small, hence the sea–air CO_2 flux is reduced significantly as indicated by the green areas in Fig. 15B. As the ice field recedes with the arrival of spring, photosynthesis draws down pCO_2 below the atmospheric level, and the open water areas become a CO_2 sink as shown in the February map (Fig. 15A).

6.3.3. *Sea–air CO_2 flux differences in the ocean basins*

The sea–air CO_2 flux is governed by the complex interactions of various oceanographic and meteorological processes. In order to gain insight in regional differences in the influences of these processes, the mean flux per unit area (t-C $month^{-1}$ km^{-2} = g-C $month^{-1}$ m^{-2}; $1t = 10^6$ g) is computed by dividing the total flux with the area for the six climatic zones in each ocean basin (Fig. 16).

The high-latitude North Atlantic (north of 50°N, Fig. 16A) is clearly the most intense CO_2 sink area on the per unit area basis. Cold temperature, strong photosynthesis, high wind speeds and high alkalinity in Arctic waters contribute at various levels over the course of the year to the intense sink.

The tropical zone 14°N–14°S for all oceans is a CO_2 source with fluxes ranging between 0.3 and 0.9 t-C $month^{-1}$ km^{-2} with small seasonal variability. The Pacific tropical zone (Fig. 16B) has the highest mean flux of 0.8 t-C $month^{-1}$ km^{-2}, the Atlantic next at 0.6 (Fig. 16A) and the Indian the lowest at 0.5 (Fig. 16C). The high Pacific flux is due primarily to an intense upwelling of CO_2-rich deep waters in the eastern half of the zone during non-El Niño periods, however, it is about 1/5 of the flux in the Arabian Sea during the peak upwelling time (July–August) (north of 14°N, Fig. 16C). This is because (a) upwelled deep waters in the northwestern Arabian Sea have much higher pCO_2 than those in the equatorial Pacific (Figs. 10B and C); (b) the gas transfer coefficient for the Arabian Sea is three times as great as that for the equatorial Pacific (Fig. 12) due to the high monsoon winds; and (c) the Pacific value is averaged over large areas including the western Warm Water zone with weak fluxes (Figs. 13 and 15).

The magnitude and seasonal amplitude of the mean area fluxes for the temperate North and South Atlantic (Fig. 16A) are similar to those for the North and South Pacific (Fig. 16B), respectively.

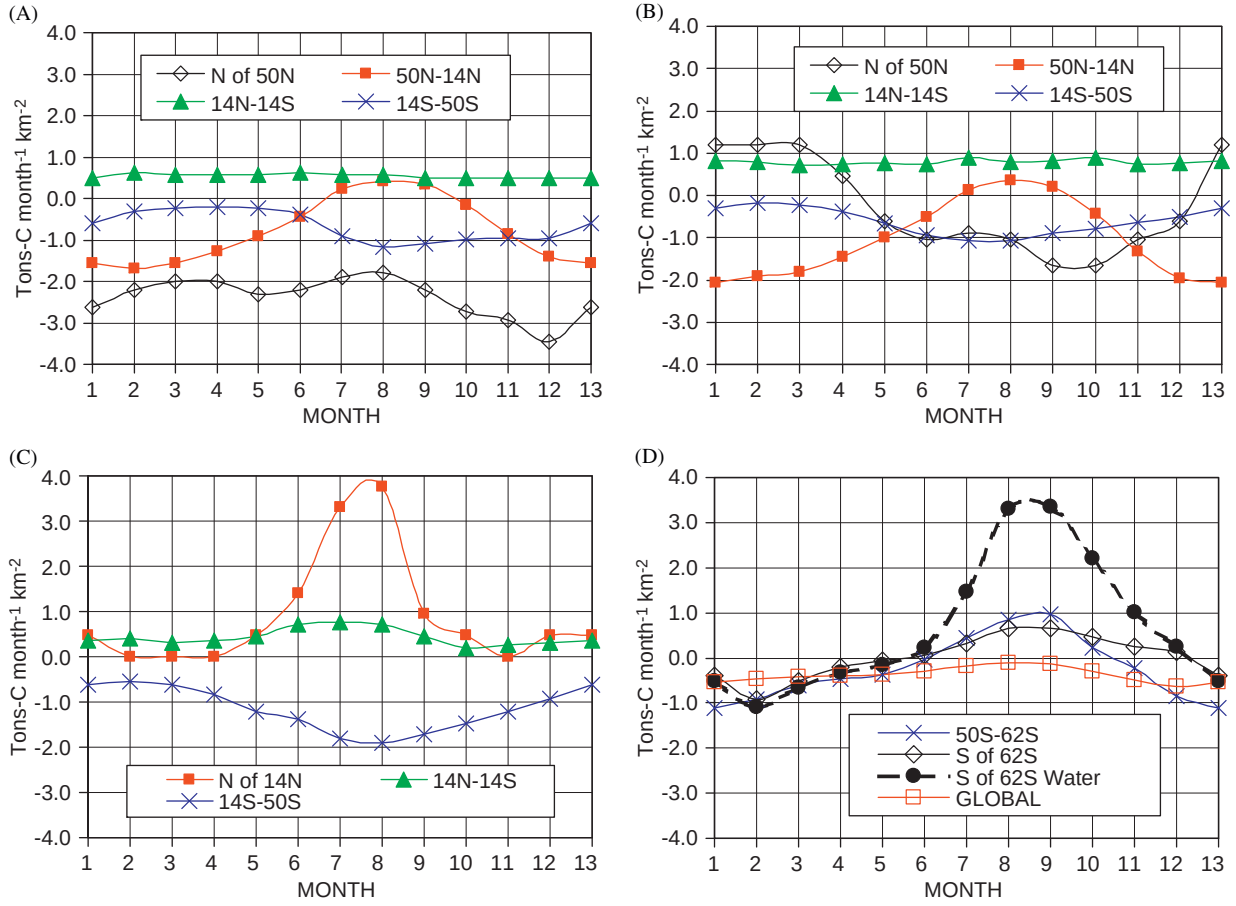

Fig. 16. Monthly mean sea–air CO_2 flux per unit area for the four major ocean basins and the global oceans in the unit of tons-carbon month^{-1} km^{-2} (1 ton = 10^6 g): (A) Atlantic, (B) Pacific, (C) Indian, and (D) Southern and Global Oceans. Month numbers 1 and 13 are January, and Month number 12 is December. For the region "South of 62°S" in panel D, the black solid curve with open diamonds indicates the flux per km^2 of geographic area including ice cover; and the black dashed curve with solid circles indicates the flux per km^2 of water exposed to the air in leads and polynyas in the ice fields. Positive values indicate sea-to-air fluxes, and negative values air-to-sea fluxes.

This suggests that the processes governing the sea–air CO_2 transfer are similar. On the other hand, the area mean air-to-sea CO_2 flux over the temperate South Indian Ocean (annual mean of −1.0 t-C month^{-1} km^{-2} for 14–50°S, Fig. 16C) is twice as intense as the corresponding regions of the Atlantic (−0.61 for 14–50°S, Fig. 16A) and Pacific (−0.56 for 14–50°S, Fig. 16B). A number of reasons may be considered. Wind speeds are higher over the South Indian Ocean (annual mean of 9.04 m s^{-1}) than the South Atlantic (annual mean of 8.48 m s^{-1}) and Pacific (annual mean speed of 8.15 m s^{-1}). Seawater pCO_2 is also lower for the South Indian Ocean (annual mean ΔpCO_2 of −16 μatm) than that for the South Atlantic (−6 μatm) and the South Pacific (−9 μatm). However, the stronger negative ΔpCO_2 in the South Indian is not well understood as discussed in Section 5.2.

The subpolar Southern Ocean between 50° and 62°S (Fig. 16D) has a sea-to-air CO_2 flux in winter and an air-to-sea flux in summer. In this zone, ΔpCO_2 is small in magnitude (Fig. 10D) ranging between +12 μatm in winter (enhanced vertical mixing) and −12 μatm in summer (biological drawdown). Although this region is mostly within the high wind speed zone (40–60°S), the flux is moderate ranging between +1 (winter) and −1 t-C month^{-1} km^{-2} (summer) because of the small ΔpCO_2 values.

The "S of 62°S" region represents the seasonal ice-field zone. Although the winter ice field extends as far north as 55°S in the Atlantic sector in some years, the northern extent of the winter sea-ice field may be located around 62°S on the average around Antarctica. Two curves are presented in Fig. 16D for this region: the black solid curve with open diamonds indicates the flux per km^2 of geographic area including ice covered areas (marked "S of 62S"); and the black dashed curve with solid circles indicates the flux per km^2 of water area exposed to the air in leads and polynyas (marked "S of 62S Water"). Water areas exposed to the air in the monthly mean ice field have been estimated using the ice cover data from the NCEP/DOE AMIP-II Reanalysis (2005). High pCO_2 in sub-ice waters (ΔpCO_2 as high as +40 μatm, Fig. 10D) accounts for the high fluxes. The differences between these curves indicate the effect of the ice cover on the flux. The high potential for CO_2 fluxes estimated for the ice field waters during Antarctic winter is similar to those for the Arabian Sea region in the North Indian Ocean during the Southwest Monsoon months. The global ocean mean uptake flux (Fig. 16D) is about 0.5 t-C month^{-1} km^{-2} with small seasonal variability.

6.3.4. *Comparison with other studies for the Southern Ocean*

The sea–air CO_2 flux and ΔpCO_2 reported for the Southern Ocean vary over a wide range due primarily to the limited number of seasonal observations over oceanographically complex areas. As discussed in Section 5.3, the larger database used for this study accounts mostly for the differences from Takahashi et al. (2002). In Table 6, the fluxes computed using the earlier database (light numbers marked 0.94 M) and the same wind speeds and gas transfer coefficients as used in this study are compared with the flux values (bold numbers marked 3.0 M). The Southern Ocean

(50–62°S) sink flux of -0.34 Pg-C y^{-1} obtained from the 0.94 M database is about six times larger than -0.06 Pg-C y^{-1} from the 3.0 M database, and this is accounted for by the improved database for ΔpCO_2.

The flux obtained in this paper is smaller than -0.17 Pg-C y^{-1} estimated by Metzl et al. (2006). Since the 3.0 M database used in this study includes the data used by Metzl et al., the flux difference is primarily attributed to the choice of the gas transfer coefficients and wind speeds. For the gas transfer coefficients, they used a scaling factor of 0.39 (Wanninkhof, 1992), while we used 0.26 (see Section 6.1). If this scaling factor is used, their flux would be reduced to about -0.1 Pg-C y^{-1}. Differences in wind speed fields used for the respective studies may account for the rest.

McNeil et al. (2007) computed seawater pCO_2 using the alkalinity (TA) and the total CO_2 concentration (TCO_2) in seawater, that were parameterized separately as a function of temperature, salinity and nutrients for each of the summer and winter seasons. They reported a CO_2 sink flux of -0.4 ± 0.25 Pg-C y^{-1} over the areas south of 50°S. The large sink flux is a result of negative ΔpCO_2, seasonally averaging about -12 μatm (seasonal range from +3 to -20 μatm) between 50° and 60°S. In contrast, our study gives a mean ΔpCO_2 of -5 μatm (seasonal range from +12 to -15 μatm) for the same zone. The discrepancy may be attributed to several reasons. First, the computed pCO_2 values depends sensitively on the accuracy of estimated values for TCO_2 and TA: in the sub-Antarctic surface waters, $(\partial \ln pCO_2/\partial \ln TCO_2)$ ranges from 12 to 15 and $(\partial \ln pCO_2/\partial \ln TA)$ from -10 to -13. The standard errors of ±8.5 μmol kg^{-1} and ±8.1 μeq kg^{-1} estimated by McNeil et al. for TCO_2 and TA, respectively should introduce a pCO_2 error of about 5% or ±15 μatm for each, and a combined error of ±20 μatm if errors in TCO_2 and TA are uncorrelated. The differences between their pCO_2 values and ours appear to be within the estimated error limit. Second, the parameterization equation for TA derived by McNeil et al. (2007) shows that TA increases with increasing nitrate concentration. On the other hand, since TA is a representation of ionic charge balance in aqueous solutions, the charge balance requires that TA should decrease with increasing nitrate concentration. Since their parameterization for TA is not consistent with the principle of ionic charge balance, it may yield biased TA values.

Le Quèrè et al. (2007) estimated the time trend of the Southern Ocean CO_2 sink intensity using an atmospheric transport model for an inversion of the atmospheric CO_2 concentration data from the Southern Ocean area. They reported that the Southern Ocean sink south of 45°S decreased significantly after 1990, and attributed this to increasing wind speeds that may cause a rise in surface water pCO_2 due to enhanced vertical mixing of deep waters as well as other associated changes in ocean biogeochemistry. Their flux trend implies that the surface water pCO_2 increased at a similar or a slightly faster rate than the mean atmospheric rate during the past 15 years. Our winter-month pCO_2 data for the Southern Ocean surface waters show an increase somewhat faster than the atmospheric pCO_2 increase rate (Table 5). The results of our analysis for the winter pCO_2 data are qualitatively consistent with their results.

6.4. Error analysis and the global sea–air CO_2 flux

The reliability of the sea–air CO_2 flux thus computed depends on the accuracy of the sea–air pCO_2 difference (ΔpCO_2) and that of the parameterization for the gas transfer coefficient and the wind speed used in it.

6.4.1. Error estimate for ΔpCO_2

One standard deviation around a mean ΔpCO_2 for $4^\circ\times5^\circ$ box is about ±10 μatm on the average over the global oceans. Since 3×10^6 measurements were made in 1630 boxes (out of a total of 1759 box areas with a $4^\circ\times5^\circ$ grid) over 12 months, the average number of measurements in each box is about 153 per month, although actual numbers vary over a wide range from one box to another. Hence, the average error for monthly mean values for seawater pCO_2 is about ±0.8 μatm ($=10/(153)^{1/2}$). The average error for the atmospheric pCO_2 (including the effect of barometric pressure) is estimated to be about ±0.2 μatm. We, therefore, estimate that the mean error for ΔpCO_2 is about ±0.9 μatm ($=(0.8^2+0.2^2)^{1/2}$). On the other hand, the gas transfer coefficient, Tr, varies from 0.03 to 0.12 g-C μatm^{-1} month^{-1} m^{-2} with an area-weighted global mean of 0.05 g-C μatm^{-1} month^{-1} m^{-2}. Using the global ocean area of 326.5×10^6 km^2, the random error for the global flux is estimated to be about ±0.2 Pg-C y^{-1} ($=0.05\times0.9$ (μatm) $\times$ 12 (months) $\times$ 326.5×10^{12} (m^2)). This corresponds to about ±13% of the net global ocean uptake flux of 1.4 Pg-C y^{-1} estimated by this study.

6.4.2. Error estimate for the sea–air gas transfer coefficient

The sea–air gas transfer piston velocity (k) and the transfer coefficient (Tr) (Eq. (8)) depends on the errors for the wind speed and the scaling factor (Γ). Although the errors in wind speeds are not well quantified, we assume a random error of ±10% for the wind speeds used in this study. The error for Γ has been estimated to be ±30% (Sweeney et al., 2007), which affects the CO_2 flux proportionally. If Γ is set at a constant value, a systematic increase in the wind speed by 10% would increase the global CO_2 flux by 20% due to the (wind speed)^2 dependence of k and Tr. Since Naegler et al. (2006) pointed out that the product {Γx [mean of (wind speed)^2]} is nearly independent of the wind speed fields used, a systematic error of +10% in wind speeds (or +20% in (wind speed)^2) should be compensated by a reduction of 20% in Γ. Therefore, the effects of systematic errors in wind speeds on the CO_2 flux are largely cancelled by corresponding changes in Γ. On the other hand, Γ is fixed at 0.26 in our study, and its ±30% (±0.42 Pg-C y^{-1}) uncertainty is largely from sources other than wind speeds. Hence, the error in Γ is considered to be uncorrelated with random errors in wind speeds.

6.4.3. Effects of the seawater pCO_2 rate of change

The sea–air pCO_2 difference and the CO_2 flux are affected by the uncertainty in the mean rate of change for surface water pCO_2 used for normalization of the data to a reference year of 2000. Since the magnitude of corrections is greater for measurements taken longer years away from the reference year, the magnitude of the effects depends on the age distribution of measurements. As seen in Table 5, while a global mean value of 1.5 μatm y^{-1} is used for the normalization of the data to a reference year 2000, the rate appears to be lower in the North Pacific and higher in the North Atlantic than the global mean by 0.3 μatm y^{-1}. Table 7 shows the sensitivity of the regional and global sea–air CO_2 flux computed for three rates of increase. For a decrease of 0.1 μatm y^{-1} for the entire global ocean, the global sea–air CO_2 flux increases by about 0.1 Pg-C y^{-1}. However, if a rate of 1.2 μatm y^{-1} is used for the Pacific and 1.8 μatm y^{-1} is used for the Atlantic, the Pacific sink flux increases by 0.1 Pg-C y^{-1} and the Atlantic sink flux decreases by 0.1 Pg-C y^{-1}. Hence the effects cancel each other and the global flux remains unaffected.

Although the geographic coverage is limited for the rate, the results in Table 5 suggest an area-weighted mean of 1.5 ± 0.5 μatm y^{-1} for the global mean. Taking this as the uncertainty for the global mean rate, we estimate an error of ±0.5 Pg-C y^{-1} (or ±35%) for the global ocean sea–air flux.

Table 7
Sensitivity of the rate of increase in surface ocean pCO_2 to the sea–air CO_2 flux.

	Latitude zones	Flux (Pg-C y^{-1})				
		Pacific[a]	Atlantic	Indian	Southern	Global[a]
Change rate	N of 50°N	−0.03	−0.28			−0.32
	50–14°N	−0.52	−0.24	0.02		−0.74
	14°N–14°S	0.45	0.08	0.09		0.62
1.2 μatm y^{-1}	14–50°S	−0.46	−0.25	−0.48		−1.19
	50–62°S				−0.10	−0.10
	S of 62°S				0.00	0.00
	Total	−0.56	−0.69	−0.37	−0.09	−1.71
Change rate	N of 50°N	−0.03	−0.27			−0.30
	50–14°N	−0.51	−0.22	0.02		−0.69
	14–14°S	0.48	0.10	0.10		0.69
1.5 μatm y^{-1}	14–50°S	−0.41	−0.29	−0.44		−1.05
	50–62°S				−0.06	−0.06
	S of 62°S				0.01	0.01
	Total	−0.46	−0.58	−0.32	−0.05	−1.41
Change rate	N of 50°N	−0.03	−0.26			−0.28
	50–14°N	−0.48	−0.20	0.03		−0.65
	14°N–14°S	0.51	0.12	0.12		0.75
1.8 μatm y^{-1}	14°S–50°S	−0.36	−0.15	−0.41		−0.92
	50–62°S				−0.03	−0.03
	S of 62°S				0.01	0.01
	Total	−0.36	−0.48	−0.26	−0.01	−1.12

Each of these rates is used to normalize the data to the reference year 2000: 1.5 μatm y^{-1} representing the global mean, and 1.2 and 1.8 μatm y^{-1} representing the mean rates observed in the North Pacific and North Atlantic, respectively. The scaling factor of 0.26 for the gas transfer rate and the NCEP-DOE-AMIP II wind speeds are used for the calculation.

[a] Exclude the Bering Sea areas where negative rates are observed.

6.4.4. Error due to undersampling

Systematic biases in surface water pCO_2 and global flux arise from undersampling and our interpolation method. This may be evaluated on the basis of a comparison of the SST values measured in this study with the extensive climatological SST data of Shea et al. (1992). The SST values measured concurrently with seawater pCO_2 are processed using the same space–time interpolation method as used for the seawater pCO_2 data. The differences between our values with the climatological mean for the corresponding months and locations are computed in a SST range from −1.9 to 30 °C and averaged (see Fig. 3 of Takahashi et al., 1997, as an example). For 21,108 pairs of comparison for monthly mean values, that include those for boxes with measurements as well as those interpolated (due to no measurements), the mean difference for (interpolated–climatological mean) is found to be +0.08 °C with a standard deviation of mean of ±0.01 °C (= (1.4 °C standard deviation)/$(21{,}108)^{1/2}$). For the interpolated boxes only ($N = 10{,}708$), the mean difference is +0.13 °C with a standard deviation of mean of ±0.02 °C (standard deviation = ±1.7 °C); and for the boxes with at least one observation ($N = 10{,}400$), the mean difference is +0.03 ± 0.01 °C (standard deviation = ±1.0 °C). Assuming that the SST biases reflect biases in calculated surface water pCO_2, and using an isochemical temperature dependence ($\partial \ln pCO_2/\partial T$) of 4.23% °$C^{-1}$ (Takahashi et al., 1993), we estimate that the global mean surface water pCO_2 obtained in this study may be biased by about +1.3 μatm (= 350 μatm × 0.0423 °C^{-1} × 0.08 °C). This corresponds to a flux bias of 20% (or 0.25 Pg-C y^{-1}) when a global mean transfer coefficient of 0.05 g-C m^{-2} μatm^{-1} month^{-1} is used. Accordingly, our global ocean uptake flux of −1.42 Pg-C y^{-1} may be biased low by about 20%, and could be as large as −1.7 Pg-C y^{-1}.

6.4.5. Error summary

In summary, the net global sea–air flux may be subject to random errors of ±0.18 Pg-C y^{-1} (±13%) from the ΔpCO_2 measurements, ±0.42 Pg-C y^{-1} (±30%) in the scaling factor for the gas transfer piston velocity parameterization, ±0.28 Pg-C y^{-1} (±20%) in wind speeds and ±0.5 Pg-C y^{-1} (±35%) for the mean rate of change in ocean water pCO_2. A combined precision for the flux is estimated to be ±0.7 Pg-C y^{-1} (= $(0.18^2+0.42^2+0.28^2+0.50^2)^{1/2}$) or ±53%. Additionally, the net global ocean uptake flux is subject to systematic biases caused by undersampling and the interpolation method used, and may be as large as −1.7 Pg-C y^{-1}. Thus, the best estimate for the climatological mean for the net CO_2 uptake by the global ocean in the reference year 2000 is −1.6 ± 0.9 Pg-C y^{-1}, which includes a possible undersampling correction applied to our direct estimate of −1.4 ± 0.7 Pg-C y^{-1}. Counting the pre-industrial steady-state sea–air CO_2 flux of 0.4 ± 0.2 Pg-C y^{-1} (Sarmiento and Sundquist, 1992; Aumont et al., 2001; Gloor et al., 2003; Bender et al., 2005; Jacobson et al., 2007a), the oceanic uptake flux of CO_2 including anthropogenic CO_2 is −2.0 ± 1.0 Pg-C y^{-1}. In this study, the dependence for the gas transfer rates is taken to be proportional to (wind speed)^2 and only one wind speed product is used. However, the estimated flux depends on the choice of this information.

7. Summary and conclusion

A climatological mean distribution for the surface water pCO_2 over the global oceans has been constructed based upon about 3 million measurements for surface water pCO_2 obtained from 1970 to 2007. The observations made in the El Niño periods over the equatorial zone of the Pacific (5°N–5°S) and in coastal waters are excluded from the analysis. The database used for this study is about three times as large as the 0.94 million used for our earlier paper (Takahashi et al., 2002). Since the surface water pCO_2 changed with time and the measurements were made over many years, the global data observed in different years have been corrected to a single virtual reference year 2000 using a mean rate of increase of 1.5 μatm y^{-1}, which is consistent with the decadal mean rate of increase in the atmospheric pCO_2. This is estimated on the basis of a time-trend analysis using deseasonalized surface water pCO_2 data in the North Atlantic, North and South Pacific and Southern Oceans. The pCO_2 values thus corrected to the reference year 2000 are binned into a 4° (latitude) × 5° (longitude) grid and interpolated in space and time using a lateral two-dimensional diffusion–advection equation (Takahashi et al., 1995, 1997), and monthly mean values for the pixels are presented. Thus, the distributions presented in this paper represent the mean non-El Niño conditions adjusted to a reference year 2000. Outside the equatorial Pacific, the effects on pCO_2 of El Niño and the Pacific Decadal Oscillations cannot be identified.

The sea–air pCO_2 difference, ΔpCO_2 is computed as [(climatological mean surface water pCO_2 for each month)—(monthly mean atmospheric pCO_2 in the year 2000)] in each box area. The atmospheric pCO_2 values are computed using the dry-air mol fraction for the year 2000 (GLOBALVIEW—CO_2, 2006) and the climatological mean values for monthly barometric pressures and sea-surface temperatures. The monthly distributions over the global oceans are presented in Figs. 9 and 10.

The rate constant for the air–sea gas transfer is parameterized as a function of (wind speed)^2. The scaling factor of 0.26 for long-term (month) mean gas transfer piston velocity is estimated by inverting the bomb ^{14}C data using Ocean General Circulation models and the 1979–2005 NCEP-DOE AMIP-II Reanalysis (R-2) wind speed data (Sweeney et al., 2007). The net sea–air CO_2 flux is

computed by multiplying the ΔpCO_2 and the gas transfer coefficient. Regional mean sea–air flux per unit area varies among the ocean basins (Fig. 16). The high-latitude North Atlantic, including the Nordic seas and portion of the Arctic Sea, is the most intense CO_2 sink area on the basis of per unit area, with an annual mean of -2.5 t-C month^{-1} km^{-2} as a result of the highly negative ΔpCO_2 (Fig. 10) and strong winds (Fig. 12). The temperate South Indian Ocean 14–50°S has an annual mean of -1.1 t-C month^{-1} km^{-2}, which is twice as intense as the corresponding regions of the Atlantic (-0.61 for 14–50°S) and Pacific (-0.56 for 14–50°S). The ice-free sub-Antarctic zone (50°S–62°S) has a small mean annual flux as a result of the summer sink flux canceling with the winter source flux. In the seasonal ice-field zone, south of 62°S, the sea-to-air CO_2 flux is very high per unit area of waters exposed to the air, but is small for the ice field area as a whole because of the ice cover. As ice fields retreat in springtime, surface waters become a strong sink due to locally intense phytoplankton blooms caused by increased sunlight and abundant nutrients in shallow, low salinity mixed layer. The mean air-to-sea flux for the global oceans is about 0.4 t-C month^{-1} km^{-2}.

The annual mean for the net sea–air CO_2 flux over the global oceans and the geographic distribution are summarized in Figs. 13–16 and in Table 5. Of the major ocean basins, the Southern Hemisphere oceans, south of 14°S to Antarctica, is the largest CO_2 sink taking up about -1.1 Pg-C y^{-1}, while the northern oceans north of 14°N take up about -0.7 Pg-C y^{-1}. The equatorial oceans, 14°N–14°S, emit +0.7 Pg-C y^{-1} to the atmosphere. The net uptake flux for the global oceans is estimated to be -1.6 ± 0.9 Pg-C y^{-1} counting uncertainties in the ΔpCO_2, scaling factor, wind speeds and rates of change in surface water pCO_2 as well as errors due to undersampling and interpolation method. Taking the pre-industrial steady-state flux value of 0.4 ± 0.2 Pg-C y^{-1} into account, the total ocean uptake flux for anthropogenic CO_2 emissions is estimated to be -2.0 ± 1.0 Pg-C y^{-1} in a reference year 2000.

Acknowledgments

We thank valuable advice and suggestions from Steve Ackley, Nikki Gruber, Doug Martinson, John Shepherd and Christopher Zappa; and constructive suggestions from two anonymous reviewers. Tobias Naegler pointed out the effect of dilution of $^{14}CO_2$ by the uptake of fossil fuel CO_2. This study has been supported by grants from many national and international government agencies and private foundations. We gratefully acknowledge for the support and encouragements from the US National Science Foundation, National Oceanographic Atmospheric Administration, Department of Energy, National Aeronautical and Space Administration, EXXON Research & Engineering Company, Ford Motor Company and David Packard Foundation, and Raytheon Antarctic Service (the United States); the European Commission (CARBOOCEAN GOCE-511176-1); The Natural Environment Research Council (the United Kingdom); the Australian Climate Change Science Program; and various government agencies and foundations of Belgium, Canada, France, Germany, Iceland, Japan, Norway and The Netherlands. Without the dedication of the sea-going staff from the participating institutions, this study would not be possible. This is a LDEO Contribution no. 7062.

References

Atlas of Surface Marine Data, 1994. CD-ROM NODC-56, Ocean Climate Laboratory. NOAA, Washington, DC.

Aumont, O., Orr, J.C., Monfray, P., Ludwig, W., Amiotte-Suchet, P., Probst, J.-L., 2001. Riverine-driven interhemispheric transport of carbon. Glob. Biogeochem. Cycles 15 (2), 393–406.

Bakker, D.C.E., de Baar, H.J.W., Bathmann, U.V., 1997. Changes of carbon dioxide in surface waters during spring in the Southern Ocean. Deep-Sea Res. II 44, 91–128.

Bakker, D.C.E., Hoppema, M., Schröder, M., Geibert, W., de Baar, H.J.W., 2008. A rapid transition from ice covered CO_2-rich waters to a biologically mediated CO_2 sink in the eastern Weddell Gyre. Biogeosci. Discuss. 5, 1205–1235 ⟨http://www.biogeosciences-discuss.net/papers_in_open_discussion.html⟩.

Bates, N.R., 2001. Interannual variability of oceanic CO_2 and biogeochemical properties in the Western North Atlantic subtropical gyre. Deep-Sea Res. II 48 (8–9), 1507–1528.

Bates, N.R., 2007. Interannual variability of the oceanic CO_2 sink on the subtropical gyre of the North Atlantic Ocean over the last 2 decades. J. Geophys. Res. 112.

Bellerby, R.G.J., Hoppema, M., Fahrbach, E., De Baar, H.J.W., Stoll, M.H.C., 2004. Interannual controls on Weddell Sea surface water fCO_2 during the autumn–winter transition phase. Deep-Sea Res. I 51, 793–808.

Bender, M.L., Ho, D.T., Hendricks, M.B., Mika, R., Bazttle, M.O., Tans, P.P., Conway, T.J., Sturtevant, B., Cassar, N., 2005. Atmospheric O_2/N_2 changes, 1993–2002: implications for the partitioning of fossil fuel CO_2 sequestration. Glob. Biogeochem. Cycles 19, GB4017.

Broecker, W.S., Takahashi, T., 1966. Calcium carbonate precipitation on the Bahama Banks. J. Geophys. Res. 71, 1575–1602.

Broecker, W.S., Peng, T.-H., Ostlund, G., Stuiver, M., 1985. The distribution of bomb radiocarbon in the ocean. J. Geophys. Res. 90, 6953–6970.

Capone, D.G., Burns, J.a., Michaels, A.F., Montoya, J.P., Subramaniam, A., Carpenter, E.J., 2005. Nitrogen fixation by *Trichodesmium* spp.: an important source of new nitrogen to the tropical and subtropical North Atlantic Ocean. Glob. Biogeochem. Cycles 19.

Chen, G.L., Peng, J.H., Xu, W.X., Goyet, C., Millero, F.J., O'Sullivan, D.W., Eischeid, G., McCue, S.J., Bellerby, R.G.J., 1998. Temporal variations of pCO_2 in surface seawater of the Arabian Sea in 1995. Deep-Sea Res. I 45, 609–623.

Corbière, A., Metzl, N., Reverdin, G., Brunet, C., Takahashi, T., 2007. Interannual and decadal variability of the carbon dioxide and air–sea CO_2 fluxes in the North Atlantic subpolar gyre. Tellus B 59, 168–179.

Donlon, C.J., Minnett, P.J., Gentemann, C., Nightingale, T.J., Barton, I.J., Ward, B., Murray, M., 2002. Toward improved validation of satellite sea surface skin temperature measurements for climate research. J. Clim. 15, 353–369.

Dore, J.E., Lukas, R., Sadler, D.W., Karl, D.M., 2003. Climate-driven changes to the atmospheric CO_2 sink in the subtrotical North Pacific Ocean. Nature 424, 754–757.

Fairall, C.W., Bradley, E.F., Godfrey, J.S., Wick, G.A., Edson, J.B., Young, G.S., 1996. Cool-skin and warm layer effects on sea surface temperature. J. Geophys. Res. 101, 1295–1308.

Feely, R.A., Boutin, J., Cosca, C.E., Dandonneau, Y., Etcheto, J., Inoue, H., Ishii, M., LeQuéré, C., Mackey, D.J., McPhaden, M., Metzl, N., Poisson, A., Wanninkhof, R., 2002. Seasonal and interannual variability of CO_2 in the equatorial Pacific. Deep-Sea Res. II 49, 2443–2469.

Feely, R.A., Takahashi, T., Wanninkhof, R., McPhaden, M.J., Cosca, C.E., Sutherland, S.C., Carr, M.-E., 2006. Decadal variability of the air–sea CO_2 fluxes in the equatorial Pacific Ocean. J. Geophys. Res. 111, C07S03.

Gentemann, C.L., Donlon, C., Stuart-Menteth, A., Wentz, F.J., 2003. Diurnal signals in satellite sea surface temperature measurements. Geophys. Res. Lett. 30, 1140.

Gibson, J.A.E., Trull, T., 1999. Annual cycle of fCO_2 under sea-ice and in open ocean water in Prydz Bay. East Antarctica. Mar. Chem. 66, 187–200.

GLOBALVIEW—CO_2, 2006. Cooperative atmospheric data integration project—carbon dioxide. CD-ROM, NOAA CMDL, Boulder, CO. [Also available on Internet via anonymous FTP to ftp.cmdl.noaa.gov, Path: ccg/co2/GLOBALVIEW].

Gloor, M., Gruber, N., Sarmiento, J., Sabine, C.L., Feely, R.A., Rodenbeck, C., 2003. A first estimate of present and preindustrial air–sea CO_2 flux patterns based on ocean interior carbon measurements and models. Geophys. Res. Lett. 30.

Gibson, J.A.E., Trull, T., 1999. Annual cycle of fCO_2 under sea-ice and in open ocean water in Prydz Bay. East Antarctica. Mar. Chem. 66, 187–200.

Gordon, A.L., Chen, C.T.A., Metcalf, 1984. Winter mixed layer entrainment of Weddell deep water. J. Geophys. Res. 89, 637–640.

Gregg, W.W., Conkright, M.E., Ginoux, P., O'Reilly, J.E., Casey, N.W., 2003. Ocean primary production and climate: global decadal changes. Geophys. Res. Lett. 30.

Gruber, N., Sarmiento, J.L., 2002. Large–scale biogeochemical–physical interactions in elemental cycles. In: Robinson, A.R., McCarthy, J., Rothschild, B.J. (Eds.), The Sea, vol. 12. Wiley, New York, pp. 337–399.

Gruber, N., Keeling, C.D., Bates, N.R., 2002. Interannual variability in the North Atlantic Ocean carbon sink. Science 298, 2374–2378.

Gurney, K.R., Law, R.M., Denning, A.S., Rayner, P.J., Pak, B., the TransCom-3L2 modelers, 2004. TransCom-3 inversion intercomparison: control results for the estimation of seasonal carbon sources and sinks. Glob. Biogeochem. Cycles 18, GB1010.

Hales, B., Chipman, D.W., Takahashi, T., 2004. High-frequency measurement of partial pressure and total concentration of carbon dioxide in seawater using microporous hydrophobic membrane contactors. Limnol. Oceanogr. Methods 2, 356–364.

Hales, B., Takahashi, T., 2004. High-resolution biogeochemical investigation of the Ross Sea, Antarctica, during the AESOPS (US JGOFS) Program. Glob. Biogeochem. Cycles 18 (3), GB3006.

Ho, D.T., Law, C.S., Smith, MJ., Schlosser, P., Harvey, M., Hill, P., 2006. Measurements of air–sea gas exchange at high wind speeds in the Southern Ocean: implications for global parameterization. Geophys. Res. Lett. 33, LI6611.

Inoue, H.Y., Matsueda, H., Ishii, M., Fushimi, K., Hirota, M., Asanuma, I., Takasugi, Y., 1995. Long-term trend of the partial pressure of carbon dioxide (pCO_2) in surface waters of the western North Pacific, 1984–1993. Tellus 47B, 391–413.

Ishii, M., Saito, S., Tokieda, T., Kawano, T., Matsumoto, K., Inoue, H.Y., 2004. Variability of surface layer CO_2 parameters in the western and central equatorial Pacific. In: Shiyomi, M., Kawahata, H., Koizumi, H., Tsuda, A., Awaya, Y. (Eds.), Global Environmental Change in the Ocean and Land. TERRAPUB, Tokyo, pp. 59–94.

Jacobson, A.R., Mikaloff-Fletcher, S.E., Gruber, N., Sarmiento, J.L., Gloor, M., 2007a. A joint atmosphere–ocean inversion for surface fluxes of carbon dioxide: 1. Methods and global-scale fluxes. Glob. Biogeochem. Cycles 21, GB1019.

Jacobson, A.R., Mikaloff-Fletcher, S.E., Gruber, N., Sarmiento, J.L., Gloor, M., 2007b. A joint atmosphere-ocean inversion for surface fluxes of carbon dioxide: 2. Regional results. Glob. Biogeochem. Cycles 21, GB1020.

Kalnay, E., Kanamitsu, M., Kistler, R., Collins, W., Deaven, D., Gandin, L., Iredell, M., Saha, S., White, G., Woollen, J., Zhu, Y., Chelliah, M., Ebisuzaki, W., Higgins, W., Janowiak, J., Mo, K.C., Ropelewski, C., Wang, J., Leetmaa, A., Reynolds, R., Jenne, Roy., Joseph, D., 1996. The NCEP/NCAR 40-year reanalysis project. Bull. Am. Meteorol. Soc. 77, 437–471.

Kanamitsu, M., Ebisuzaki, W., Woollen, J., Yang, S.-K., Hnilo, J.J., Fiorino, M., Potter, G.L., 2002. NCEP-DOE AMIP-II reanalysis (R-2). Bull. Am. Meteorol. Soc. 83, 1631–1643 The updated data to 2005 were downloaded on 22 March 2005 from 〈ftp://ftp.cdc.noaa.gov/Datasets/ncep.reanalysis2/gaussian.grid/〉.

Keeling, C.D., Rakestraw, N.W., Waterman, L.S., 1965. Carbon dioxide in surface waters of the Pacific Ocean, 1. Measurements of the distribution. J. Geophys. Res. 70, 6087–6098.

Keeling, R.F., Garcia, H., 2002. The change in oceanic O_2 inventory associated with recent global warming. Proc. US Natl. Acad. Sci. 99, 7848–7853.

Keeling, C.D., Brix, H., Gruber, N., 2004. Seasonal and long-term dynamics of the upper ocean carbon cycle at Station ALOHA near Hawaii. Glob. Biogeochem. Cycles 18, GB4006.

Körtzinger, A., Send, U., Lampitt, R.S., Hartman, S., Wallace, D.W.R., Karstensen, J., Villagarcia, M.G., Llinas, O., DeGrandpre, M.D., 2008. The seasonal pCO_2 cycle at 49°N/16.5°W in the northeast Atlantic Ocean and what it tells us about biological productivity. J. Geophys. Res. 113, C04020.

Lefèvre, N., Watson, A.J., Olsen, A., Rios, A., Perez, F.F., Johannessen, T., 2004. A decrease in the sink for atmospheric CO_2 in the North Atlantic. Geophys. Res. Lett. 31, L07306.

Lenton, A., Matear, R.J., Tilbrook, B., 2006. Design of an observational strategy for quantifying the Southern Ocean uptake of CO_2. Glob. Biogeocehm. Cycles 20, GB4010.

Le Quéré, C., Rodembeck, C., Buitenhuis, E., Conway, T., Langenfelds, R., Gomez, A., Labuschagne, C., Ramonet, M., Nakazawa, T., Metzl, N., Gillett, N., Heimann, M., 2007. Saturation of the Southern Ocean CO_2 sink due to recent climate change. Science 316, 1735–1738.

Li, Z., Adamec, D., Takahashi, T., Sutherland, S.C., 2005. Global autocorrelation scales of the partial pressure of oceanic CO_2. J. Geophys. Res. 110, C08002.

Liss, P.S., Merlivat, L., 1986. Air–sea gas exchange rates: introduction and synthesis. In: Buat-Menard, P. (Ed.), The Role of Air–Sea Exchange in Geochemical Cycling. D. Reidel Publishing Co., Holland, pp. 113–127.

McGillis, W., Wanninkhof, R., 2006. Aqueous CO_2 gradients for air–sea flux estimates. Mar. Chem. 98, 100–108.

McNeil, C.L., Merlivat, L., 1996. The warm oceanic surface layer: implications for CO_2 fluxes and surface gas measurements. Geophys. Res. Lett. 23, 3575–3578.

McNeil, B.I., Metzel, N., Key, R.M., Matear, R.J., Corbiere, 2007. An empirical estimate of the Southern Ocean air–sea CO_2 flux. Glob. Biogeochem. Cycles 21, GB3011.

Metzl, N., Poisson, A., Louanchi, F., Brunet, C., Schauer, B., Bres, B., 1995. Spatio–temporal distributions of air–sea fluxes of CO_2 in the Indian and Antarctic Oceans: a first step. Tellus 47B, 56–69.

Metzl, N., Tilbrook, B., Poisson, A., 1999. The annual fCO_2 cycle and the air–sea CO_2 flux in the sub-Antarctic Ocean. Tellus 51B, 849–861.

Metzl, N., Brunet, C., Jabaud-Jan, A., Poisson, A., Schauer, B., 2006. Summer and winter air–sea CO_2 fluxes in the Southern Ocean. Deep-Sea Res. I 53, 1548–1563.

Midorikawa, T., Nemoto, K., Kamiya, H., Ishii, M., Inoue, H.Y., 2005. Persistently strong oceanic CO_2 sink in the western subtropical North Pacific. Geophys. Res. Lett. 32 (5), L05612.

Mikaloff-Fletcher, S.E., et al., 2006. Inverse estimates of anthropogenic CO_2 uptake, transport, and storage by the ocean. Glob. Biogeochem. Cycles 20, GB2002.

Naegler, T., Ciais, P., Rogers, K., Levin, I., 2006. Excess radiocarbon constrains on air-sea gas exchange and uptake of CO_2 by the oceans. Geophys. Res. Lett. 33, LI1802.

NCEP Reanalysis data, 2001. NCEP/NCAR reanalysis monthly means and other derived variables, provided by the NOAA-CIRES Climate Diagnostics Center, Boulder, CO 〈http://www.cdc.noaa.gov/cdc/data/ncep.reanalysis.derived.html〉.

NCEP/DOE 2 Reanalysis data, 2005. Ice field data provided by NOAA/OAR/ESRL PSD, Boulder, CO, via web site: 〈http://www.cdc.noaa.gov/cdc/data.ncep.reanalysis2.gaussian.html〉.

Nightingale, P.D., Malin, G., Law, C.S., Watson, A.J., Liss, P.S., Liddicoat, M.I., Boutin, J., Upsill-Goddard, R.C., 2000. In situ evaluation of air-sea gas exchange parameterizations using novel conservative and volatile tracers. Glob. Biogeochem Cycles 14, 373–387.

Nomura, D., Yoshikawa-Inoue, H., Toyota, T., 2006. The effect of sea-ice growth on air–sea CO_2 flux in a tank experiment. Tellus 58B, 418–426.

Olsen, A., Omar, A.M., Bellerby, R.G.J., Johannessen, T., Ninnemann, U., Brown, K.R., Olsson, A., Olafsson, J., Nondal, G., Kivimae, C., Kringstad, S., Neil, C., Olafsdottir, S., 2006. Magnitude and origin of the anthropogenic CO_2 increase and ^{13}C Suess effect in the Nordic seas since 1981. Glob. Biogeochem. Cycles 20, BG3027.

Omar, A., Johannessen, T., Kaltin, S., Olsen, A., 2003. The anthropogenic increase of oceanic pCO_2 in Barents Sea surface waters since 1967. J. Geophys. Res. 108, C12.

Omar, A.M., Olsen, A., 2006. Reconstructing the time history of the air–sea CO_2 disequilibrium and its rate of change in the eastern subpolar North Atlantic, 1972–1989. Geophy. Res. Lett. 33, L04602.

Oudot, C., Ternon, J.F., LeComte, J., 1995. Measurements of atmospheric and oceanic CO_2 in the tropical Atlantic: 10 years after 1982–1984 FOCAL cruises. Tellus 47B, 70–85.

Patra, P.K., Maksyutov, S., Ishizawa, M., Nakazawa, T., Takahashi, T., Ukita, J., 2005. Interannual and decadal changes in the sea–air CO_2 flux from atmospheric CO_2 inverse modeling. Glob. Biogeochem. Cycles 19, GB4013.

Quay, P., Sommerup, R., Westby, T., Sutsman, J., McNichol, A., 2003. Changes in the $^{13}C/^{12}C$ of dissolved inorganic carbon in the ocean as a tracer of anthropogenic CO_2 uptake. Glob. Biogeochem. Cycles 17 (1).

Reynolds, R.W., Smith, T.M., 1994. Improved global sea surface temperature analyses using optimum interpolation. J. Clim. 7, 929–948.

Reynolds, R.W., Rayner, N.A., Smith, T.M., Stokes, D.C., Wang, W., 2003. An improved in situ and satellite SST analysis for climate. J. Clim. 15, 1609–1625 doi:10.1175/1520-0442(2002)015〈1609:AIISAS〉2.0.CO2 (NOAA optimum interpolation (OI) sea surface temperature (SST) V2, 〈ftp://ftpprd.ncep.noaa.gov/pub/cmd/sst/papers/oiv2pap/〉).

Robertson, J.E., Watson, A.J., 1992. Thermal skin effect of the surface ocean and its implications for CO_2 uptake. Nature 358, 738–740.

Rubin, S.I., Takahashi, T., Chipman, D.W., Goddard, J.G., 1998. Primary production and nutrient utilization ratios in the Pacific sector of the Southern Ocean based on seasonal changes in seawater chemistry. Deep-Sea Res. I 45, 1211–1234.

Sabine, C.L., Feely, R.A., Gruber, N., Key, R.M., Lee, K., Bullister, J.L., Wanninkhof, R., Wong, C.S., Wallace, D.W.R., Tilbrook, B., Peng, T.-H., Kozyr, A., Ono, T., Rios, A.F., 2004. The oceanic sink for anthropogenic CO_2. Science 305, 367–371.

Sarmiento, J.L., Sundquist, E.T., 1992. Revised budget for the oceanic uptake of anthropogenic carbon dioxide. Nature 356, 589–593.

Sarmiento, J.L., Monfray, P., Maier-Reimer, E., Aumont, O., Murnane, R.J., Orr, J.C., 2000. Sea–air CO_2 fluxes and carbon transport: a comparison of three ocean general circulation models. Glob. Biogeochem. Cycles 14, 1267–1281.

Saunders, P.M., 1967. The temperature at the ocean–air interface. J. Atmos. Sci. 24, 269–273.

Schuster, U., Watson, A.J., 2007. A variable and decreasing sink for atmospheric CO_2 in the North Atlantic. J. Geophys. Res. 112, C11006.

Shea, D.J., Trenberth, K.E., Reynolds, R.W., 1992. A global monthly sea surface temperature climatology. J. Clim. 5, 987–1001.

Simmonds, I., Jacka, T.H., 1995. Relationships between the interannual variability of Antarctic sea ice and the Southern Oscillation. J. Clim. 8, 637–647.

Stoll, M.H.C., de Baar, H.J.W., Hoppema, M., Fahrbach, E., 1999. New early winter fCO_2 data reveal continuous uptake of CO_2 by the Weddell Sea. Tellus 51B, 679–687.

Sweeney, C., Smith, W.O., Hales, B., Bidigare, R.R., Carlson, C.A., Codispoti, L.A., Gordon, L.I., Hansell, D., Millero, F.J., Park, Mi.-O.K., Takahashi, T., 2000. Nutrient and carbon removal ratios and fluxes in the Ross Sea, Antarctica. Deep-Sea Res. II 47, 3395–3421.

Sweeney, C., 2003. The annual cycle of surface CO_2 and O_2 in the Ross Sea: a model for gas exchange on the continental shelves of Antarctica. In: DiTullio, G.R., Dunbar, R.B. (Eds.), Biogeochemistry of the Ross Sea, vol. 78. Antarctic Research Series, pp. 295–312.

Sweeney, C., Gloor, E., Jacobson, A.R., Key, R.M., McKinley, G., Sarmiento, J.L., Wanninkhof, R., 2007. Constraining global air–sea gas exchange for CO_2 with recent bomb ^{14}C measurements. Glob. Biogeochem. Cycles 21, GB2015.

Takahashi, T., 1961. Carbon dioxide in the atmosphere and in the Atlantic Ocean water. J. Geophys. Res. 66, 477–494.

Takahashi, T., Olafsson, J., Goddard, J., Chipman, D.W., Sutherland, S.C., 1993. Seasonal variation of CO_2 and nutrients in the high-latitude surface oceans: a comparative study. Glob. Biogeochem. Cycles 7, 843–878.

Takahashi, T., Takahashi, T.T., Sutherland, S.C., 1995. An assessment of the role of the North Atlantic as a CO_2 sink. Philos. Trans. R. Soc. London B 348, 143–152.

Takahashi, T., Feely, R.A., Weiss, R., Wanninkhof, R.H., Chipman, D.W., Sutherland, S.C., Takahashi, T.T., 1997. Global air–sea flux of CO_2: an estimate based on measurements of sea–air pCO_2 difference. Proc. Natl. Acad. Sci. 94, 8292–8299.

Takahashi, T., Sutherland, S.C., Sweeney, C., Poisson, A., Metzl, N., Tillbrook, B., Bates, N., Wanninkhof, R., Feely, R.A., Sabine, C., Olafsson, J., Nojiri, Y., 2002. Global sea–air CO_2 flux based on climatological surface ocean pCO_2, and seasonal biological and temperature effects. Deep-Sea Res. II 49, 1601–1622.

Takahashi, T., Sutherland, S.C., Feely, R.A., Cosca, C., 2003. Decadal variation of the surface water pCO_2 in the western and central Equatorial Pacific. Science 302, 852–856.

Takahashi, T., Sutherland, S.C., Feely, R.A., Wanninkhof, R., 2006. Decadal change of the surface water pCO_2 in the North Pacific: a synthesis of 35 years of observations. J. Geophys. Res. 111, C07S05.

Takahashi, T., Sutherland, S.C., Kozyr, A., 2008. Global ocean surface water partial pressure of CO_2 database: measurements performed during 1968–2006

(Version 1.0). ORNL/CDIAC-152, NDP-088. Carbon Dioxide Information Analysis Center, Oak Ridge National Laboratory, US Department of Energy, Oak Ridge, TN, 20pp.
Thiele, G., Roether, W., Schlosser, P., Kuntz, R., Siedler, G., Stramma, L., 1986. Baroclinic flow and transient-tracer fields in the Canary-Cape Verde Basin. J. Phys. Ocean. 16, 814–826.
Toggweiler, J.R., Dixon, K., Bryan, K., 1989. Simulations of radiocarbon in a coarse resolution world ocean model I: steady state pre-bomb distributions. J. Geophys. Res. 94, 8217–8242.
Wanninkhof, R., 1992. Relationship between wind speed and gas exchange. J. Geophys. Res. 97, 7373–7382.
Wanninkhof, R., McGillis, W.M., 1999. A cubic relationship between gas transfer and wind speed. Geophys. Res. Lett. 26, 1889–1892.
Wanninkhof, R.H., Sullivan, K.F., Top, Z., 2004. Air–sea gas transfer in the Southern Ocean. J. Geophys. Res. 109 (C8), C08S19.
Wanninkhof, R., 2007. The impact of different gas exchange formulations and wind speed products on global air–sea CO_2 fluxes. In: Garbe, C.S., Handler, R.A., Jähne, B. (Eds.), Transport at the Air Sea Interface: Measurements, Models and Parameterizations. Springer, Heidelberg, p. 320.
Ward, B., Wanninkhof, R., McGillis, W.R., Jessup, A.T., DeGrandpre, M.D., Hare, J.E., Edson, J.B., 2004. Biases in the air–sea flux of CO_2 resulting from ocean surface temperature gradients. J. Geophys. Res. 109, C8S08.
Weiss, R.F., 1974. Carbon dioxide in water and seawater: the solubility of a non-ideal gas. Mar. Chem. 2, 203–215.
Weiss, R.F., Price, B.A., 1980. Nitrous oxide solubility in water and seawater. Mar. Chem. 8, 347–359.
Yuan, X., Martinson, D.G., 2000. Antarctic sea ice extent variability and its global connectivity. J. Clim. 13, 1697–1717.
Zhang, X., Cai, W.-J., 2007. On some biases of estimating the global distribution of air–sea CO_2 flux by bulk parameterization. Geophys. Res. Lett. 34, L01608.